INORGANIC CHEMISTRY
FRONTIERS

REVIEW

View Article Online
View Journal | View Issue

Cite this: *Inorg. Chem. Front.*, 2023, **10**, 4650

Recent progress in ammonia synthesis based on photoelectrocatalysis

Pengyan Li,[a] Yumin Liu,[a] Muhammad Asim Mushtaq[a,b] and Dongpeng Yan *[a,b]

Photoelectrocatalytic (PEC) ammonia synthesis from nitrogen and water is a promising approach for energy development and N-neutralization goal under mild conditions. Although significant progress has been made in the past few decades, the mechanisms underlying the synergistic effect between light and electricity are still challenging. One particular line of study is to improve the performances of PEC catalysts, such as selectivity, yield, and stability, *etc*. Here we review the recent progress in PEC ammonia synthesis. We first provide a systematic description of the driven bias in PEC ammonia processes, involving electrochemical apparatus, photovoltaic voltage, and chemical potential. The various strategies, including vacancy engineering, ion doping, frustrated Lewis pair design, heterojunction construction, cocatalyst loading and single atom synthesis to fabricate new catalysts, are then outlined. The performance and mechanism of PEC N_2 reduction are further summarized, followed by the current challenge and future prospects. This would guide both the productiveness and mechanism of NH_3 synthesis based on advanced PEC systems.

Received 13th April 2023,
Accepted 18th June 2023

DOI: 10.1039/d3qi00683b

rsc.li/frontiers-inorganic

1. Introduction

Ammonia synthesis provides an effective pathway to obtain fertilizers, medicines, chemicals and explosives from air, which is significant to human survival and industrial development.[1,2] In nature, microorganisms depend on Mo–Fe protease to achieve the conversion of atmospheric N_2 to multipurpose NH_3.[3] However, azotase is extremely sensitive to environmental

[a]*Beijing Key Laboratory of Energy Conversion and Storage Materials, College of Chemistry, and Key Laboratory of Radiopharmaceuticals, Ministry of Education, Beijing Normal University, Beijing 100875, People's Republic of China*
[b]*State Key Laboratory of Chemical Resource Engineering, Beijing University of Chemical Technology, Beijing, 100029, People's Republic of China.*
E-mail: yandp@bnu.edu.cn

Pengyan Li

Pengyan Li received her M.S. degree in Chemical Engineering from North China University of Science and Technology in 2020. She is now pursuing her Ph.D. degree at Beijing Normal University under the supervision of Prof. Dongpeng Yan. Her research interest is focused on energy and environmental catalysis by photo(electro)catalytic technology, such as CO_2 reduction, water splitting, N_2 reduction, and degradation of dye.

Yumin Liu

Yumin Liu earned her Ph.D. degree (2021) in Chemical Engineering from Tianjin University for research on pharmaceutical crystallisation under the supervision of Prof. Jingkang Wang and Prof. Junbo Gong. In 2017–2019, she joined the Crystal Chemistry and Particle Process Engineering (CCAPPE) research group at the University of Manchester, UK, as a visiting Ph.D. student. During this period, she studied crystal growth and worked with Prof. Roger Davey and Dr Aurora Cruz-Cabeza. She currently works as a Postdoc fellow with Prof. Dongpeng Yan at Beijing Normal University and focuses on functional molecular materials.

oxygen, so the evolution of rhizobium cultivation technology became the key to industrialization of biological N_2-fixing. As a paragon of artificial nitrogen fixation, the Haber–Bosch (H–B) reaction has contributed to the global economy in which Fe-based compounds show excellent catalytic performances under harsh conditions (temperatures: 300–500 °C, pressures: 150–300 atm) with N_2 and H_2 as feed gases. However, catalytic N_2 hydrogenation consumes mass heat, and the production of feedstock H_2 derived from methane steam reforming results in serious carbon emissions with more than 1% of global emissions,[4] furthermore, the whole H–B craft requires a large plant infrastructure. Therefore, it is essential to find alternative approaches for sustainable N-neutralization under ambient conditions.[5–10] Electrocatalysis and/or photocatalysis has become one of the promising strategies for realizing the N cycle due to its cost advantage, environmental friendliness, and significant N_2 conversion efficiency.

Electrocatalytic N_2 reduction in water involves electron-coupled proton transfer along with various product distributions (NH_3, N_2H_2, N_2H_4, and H_2).[11–13] Generally, the bias can induce the first electron transfer progress ($N_2 + e^- \leftrightarrow N_2^-$: −3.37 V *vs.* RHE, pH = 14) and the first-H addition reaction ($N_2 + H^+ + e^- \leftrightarrow N_2H^+$: −3.20 V *vs.* RHE) that are not favourable thermodynamically, and accomplish continuously the following reduction.[14,15] However, the deficient sites and hydrogen evolution reaction (HER) result in minimal yield and low Faradaic efficiency (FE) in electrocatalytic ammonia synthesis.[16–19] Most studies have proved that Bi-based materials and layered double hydroxides (LDHs) have the ability to undergo photocatalytic N_2 reduction even if the band structures do not meet the requirements of the first electron transfer and the first-H addition, which contribute to considerable N_2 activation, accelerated charge separation, and desired electron generation with strong reducibility.[20] Currently, the integration of electrocatalysis and photocatalysis serves as an effective way to improve the yield and selectivity of NH_3 by virtue of the bias of electrocatalysis and the abundant sites of photocatalysts (Fig. 1).[21–23]

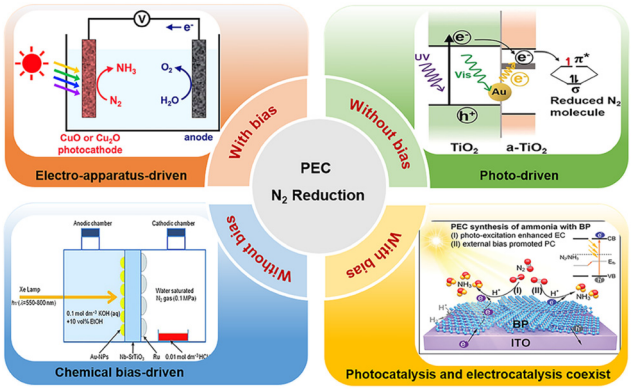

Fig. 1 Schematic diagram of multiform PEC nitrogen fixation driven by an external bias, solar energy, chemical potential under irradiation, and coexistence of photocatalytic and electrocatalytic N_2 reduction.

PEC N_2 reduction is a process in which catalysts are excited under irradiation to generate carriers, and then carriers are

Muhammad Asim Mushtaq

Muhammad Asim Mushtaq received his Master's degree in 2015 from the University of Engineering and Technology Lahore, Pakistan. He obtained his Ph.D. degree in Chemical Engineering and Technology (2021) from Beijing University of Chemical Technology (BUCT), PR China. Recently, he joined as a Postdoc fellow at Shenzhen University, Guangdong, PR China. He worked under the supervision of Prof. Dongpeng Yan and Prof. Shengfu Ji at the Beijing Key Laboratory of Energy Conversion and Storage Materials, Beijing Normal University (BNU), and the State Key Laboratory of Chemical Resource Engineering, BUCT, PR China. His research focuses on the design and synthesis of catalytic materials for photo/electrochemical catalysis.

Dongpeng Yan

Dongpeng Yan obtained his Ph.D. degree under the supervision of Prof. Acad. Xue Duan from Beijing University of Chemical Technology (BUCT, China) in 2012. Then, he became an associate professor at BUCT. In 2014, he moved to Beijing Normal University (China) as a full professor. In 2011 and 2013, as a visiting scholar, he studied at the University of Cambridge (UK) and University College London (UK). His research topics are functional molecular materials, host–guest chemistry, and photo-electrochemistry. He has received the Tang Aoqing Chemical Scholarship (2011) and the Outstanding Doctoral Dissertation Prize in Beijing (2013) amongst others. His interest focuses on the chemistry of functional materials and photo(electro)catalysis. As a corresponding author, he has published more than 150 scientific papers (such as in Chem. Soc. Rev., Angew. Chem., JACS, Adv. Mater. *and* Nature Commun.*). He was awarded the Newton Advanced Fellowship of Royal Society and the Royal Society of Chemistry Fellowship*

separated into electrons and holes, finally, electrons migrate rapidly and participate in N_2 reduction on the surface sites assisted with the bias. In addition, the photoelectric synergy is reflected in the coexistence of photochemical and electrochemical reactions. Therefore, PEC NH_3 synthesis is considered as a promising approach that possesses advantages from photocatalysis and electrocatalysis simultaneously to efficiently complete N_2 conversion.[24–26] A classical double chamber contains a photocathode (*i.e.* catalysts), anode (*i.e.* counter electrode), electrolyte, N_2 and proton exchange membrane for PEC N_2 fixation. Candidate photocathodes include inorganic semiconductors with suitable bandgaps (g-C_3N_4, BiOI, TiO_2, Cu_2O, $W_{18}O_{49}$)[27,28] and metal modifications,[29,30] metal–organic frameworks with adjustable structures,[31] and single atoms with remarkable active sites.[32] In consideration of the fact that the more negative position of the conduction band (CB) minimum and the enhanced capacity of electron reduction are favourable to N_2 reduction in the PEC strategy, vacancy engineering, heteroatom-doping, heterostructure construction, and single atom synthesis are promising approaches to improve N_2 reduction ability. What's more, the extended light response capacity to the near-infrared region is a potential idea for solar-based economy in PEC N_2 reduction.[33,34]

Chemisorption is a crucial step for N_2 reduction because appropriate adsorption can destroy the molecular symmetry and enhance the proton affinity,[35] thus promoting N_2 hydrogenation. However, the bond energy (941 kJ mol^{-1}) and cleavage energy (410 kJ mol^{-1}) indicate that N_2 activation is challenging (Fig. 2a). Many studies have investigated activation mechanisms, such as vacancy engineering,[27,36] large specific surface area, transition metal (TM)/non-metal doping,[25] and thermal field coupling. The empty d orbital of the TMs can capture lone pair electrons from N_2, and the occupied d orbital donates electrons to the π^* orbital, thus producing a weak N≡N bond through the 'acceptor–donor' route.[37] In addition to metals, B-based molecules with empty orbitals and lone pair electrons have similar electronic structures to TMs, so N_2 activation could be achieved through the 'acceptor–donor' pathway of B-containing catalysts (Fig. 2b and c).[37–40]

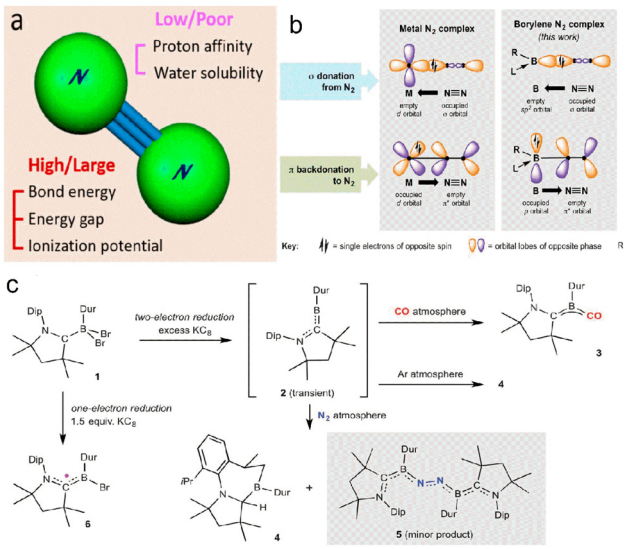

Fig. 2 (a) N_2 molecular structure,[41] Copyright 2020, American Chemical Society. (b) Mechanism of metal activation N_2 (left) and boron activation N_2 (right), (c) Outcomes of various reduction reactions of dihaloborane adduct **1**, including generation of a transient dicoordinate borylene species (**2**) and its reactionwith dinitrogen. Dip, 2,6-diisopropylphenyl; Dur, 2,3,5,6-tetramethylphenyl.[38] Copyright 2018, American Association for the Advancement of Science.

The research studies of electrocatalytic and photocatalytic ammonia synthesis are flourishing;[42–45] however, systematic summarizations of PEC N_2 reduction are rather rare. Here, we review the various bias-driven photocatalytic ammonia processes, involving electrochemical apparatus, photovoltaic voltage and chemical potential. The various strategies and mechanistic understanding based on calculations and experiments are then outlined, furthermore, we summarize the methods of NH_3 quantification, and highlight the necessity of nitrogen source determination.

2. Merging the solar strategy and the electrical strategy for PEC N_2 reduction

There are synergistic effects between light and electricity, which promote the PEC progress by taking advantage of both photocatalysis and electrocatalysis.[46,47] In particular, the electrocoupled photocatalysis strategy avoids NH_3 oxidation, enhances the reduction ability of electrons, and boosts the carrier separation capacity, while photo-assisted electrocatalysis is more outstanding than single electrocatalysis progress, which contributes to the equilibrium of electron distribution under irradiation.[48] Besides, the synergistic effect is displayed in the form of the coexistence of photochemical and electrochemical processes, that is, the potential of electrons is determined by bias in electrocatalysis, and the reduction ability of photoelectrons depends on the minimum CB of semiconductors for photocatalysis.[49]

2.1 PEC N_2 reduction assisted by electrochemical apparatus

Generally, in the PEC process, light is absorbed to initiate the catalytic reaction directly, and the applied bias is used to promote the migration of the photogenerated electrons by changing the band bending.[49–51] Upon quenching photogenerated holes located on the valence band (VB),[52] regulating the H^+ concentration on the surface of the catalyst,[27] and increasing the accumulation of electrons in the catalytic site, the catalytic performance of ammonia synthesis would be significantly improved. Electrocatalysis enhanced by photo-excitation and photocatalysis promoted by external bias occur simultaneously in PEC N_2 reduction, which make the catalysis more effective than the individual electrocatalytic or photocatalytic nitrogen fixation. It was reported that black phosphorus on indium tin oxide showed extraordinary PEC N_2 reduction properties, which benefit from the coexistence of electrocatalysis and photocatalysis.[48]

2.2 Solar-driven and chemical bias-driven PEC N_2 reduction

Photocatalysts (such as g-C_3N_4, TiO_2, $BiVO_4$, *etc.*) exhibit inefficient electrocatalytic performance due to poor conductivity, and there is a obvious side reaction (HER) for the electrochemical apparatus-assisted PEC strategy. The current studies have proved that PEC N_2 fixation can be carried out without electrochemical apparatus, and the formed anode photovoltage contributes negative potential to N_2 reduction in the form of compensation voltage.[53–55] The photovoltage from plasma-induced semiconductors shows huge potential for efficient ammonia synthesis in PEC cells without apparatus. Ali *et al.* described a solar-driven PEC cell over plasmon-assisted Si for atmospheric N_2 reduction and produced a high yield (13.3 mg m^{-2} h^{-1}) under 2 sun radiation for the first time.[22] Lee *et al.* reported that the photovoltage generated from Au modified ordered Si nanoarrays can reduce nitrate to ammonia with a FE of 95.6% at 0.2 V *vs.* RHE.[56] Li *et al.* fabricated a photovoltaic cell to realize PEC N_2 fixation with a high NH_3 yield (at the level of μmol h^{-1} or even mmol h^{-1}) over the TiO_2/Au photocathode.[57] Inspired by the successful construction of Au-loaded black silicon, Wu's group synthesized Ag-loaded black silicon for PEC nitrogen fixation without external bias,[25] and the catalysts achieved a high FE (40.6%) and NH_3 yield (2.87 μmol h^{-1} cm^{-2}). The perovskite-based photocathode (TiO_x/CdS/Cu_2ZnSnS_4) achieved NH_3 production from NO_3^- reduction with a FE of 89.1% (Fig. 3).[58]

Photocatalytic N_2 fixation is completed under the action of chemical bias induced by pH. Oshikiri's group was committed to research chemical bias-driven PEC N_2 fixation over Au/$SrTiO_3$ to improve NH_3 selectivity.[30,59] The photo-excited hot electrons from Au were transferred to the CB of $SrTiO_3$ to induce nitrogen reduction, and resulted in a hole on the $SrTiO_3$ surface for the oxidation reaction. There is an accelerated reaction under the action of chemical bias that was generated when the anode potentials move negatively and the cathode potentials move positively.

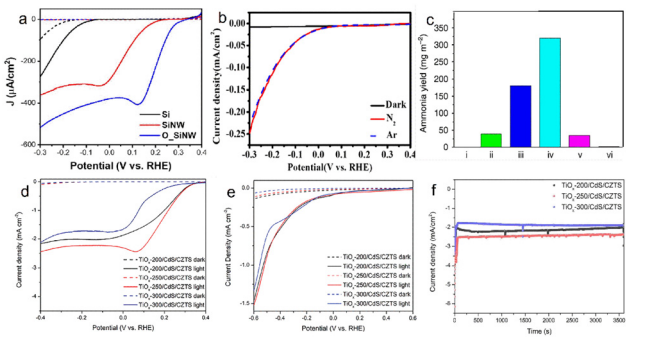

Fig. 3 The enhanced current density or improved NH_3 yield under light irradiation compared to that in the dark. (a) *J*–*V* plots of planar Si (black), Si nanowire (red), and highly ordered Si nanowire (blue) photocathodes for NO_3^- reduction in Ar-filled K_2SO_4 with KNO_3. Dashed lines represent dark current,[56] Copyright 2022, Wiley-VCH. (b) ammonia yield on various substrates: (i) P-type Si, (ii) black Si, (iii) Au/black Si, (iv) Au/black Si/Cr, and (v) Au/Si/Cr under photo-radiation, (vi) Au/black Si/Cr under dark conditions,[22] Copyright 2016, Nature Publishing Group. (c) Linear sweep voltammetry (LSV) of the Ag/black Si electrode under N_2, Ar and dark conditions,[25] Copyright 2020, American Chemical Society. (d) The LSV of TiO_x/CdS/Cu_2ZnSnS_4 in KNO_3 and H_2SO_4 solution, (e) the LSV of TiO_x/CdS/Cu_2ZnSnS_4 and in K_2SO_4 solution, (f) the chronoamperometry curves of TiO_x/CdS/Cu_2ZnSnS_4 with different spray coating temperatures at 0 V *vs.* RHE.[58] Copyright 2022, Wiley-VCH.

3. Synthesis and performance of advanced catalysts for PEC N_2 reduction

3.1 Vacancy engineering

Thermal vibration may cause atoms to deviate from the equilibrium position or escape from the surface lattice, and form vacancies.[60] As one of the most common defects on atomic-scale surfaces, vacancies can promote charge separation, anchor single atoms, and act as adsorption sites by breaking N≡N.[61–63] Therefore, the creation of vacancies significantly improved PEC performance for ammonia synthesis.

The methods for constructing oxygen vacancies have been widely studied, and the nitrogen fixation performance has been significantly improved. BiOF, BiOCl, BiOBr and BiOI are metallic compounds consisting of a $[Bi_2O_2]^+$ layer and a F/Cl/Br/I atomic layer through Van Der Waals interaction. The induced dipole action between the layered structures is favourable to form an electric field, thus passivating the recombination of photogenerated carriers.[65] Due to improved electronic availability, the O_{vs} located on the BIOX (X = F, Cl, Br, I) surface is used as a reaction site to facilitate N_2 reduction.[66] Bai *et al.* synthesized O_{vs}-BiOI photocathodes by the *in situ* electrodeposition method (Fig. 4a),[24] and the adsorption capacity of R-BiOI to N_2 was significantly enhanced after introducing O_{vs} (Fig. 4b). The ammonia production rate is 1400 μmol m^{-2} h^{-1} (Fig. 4c) at 0.4 V *vs.* RHE, which is 1.3 times higher that of the anaerobic catalyst. Similarly, Lin *et al.* prepared an O_{vs}-BiOBr/TiO_2 photoelectrode, and the O_{vs} elevated the capacity of capturing photoelectrons. The bandgap of O_{vs}-BiOBr was reduced to 2.76 eV, indicating that O_{vs} can broaden the light absorption range (Fig. 4d). The O_{vs} is in favor of the formation of quasi-continuous defects that transport electrons under low-energy light irradiation, and O_{vs}-BiOBr/TiO_2 increases the NH_3 yield, which is 3.3 fold of the BiOBr/TiO_2 photocathode.[27] Mao *et al.* prepared Li$xMoO_3$ nanosheets with O_{vs} through the lithiation strategy, and there are more abundant O_{vs} and Mo^{5+} in Li$xMoO_3$ than in MoO_3 (Fig. 4e).[64] Density functional theory (DFT) calculations confirmed that Li$xMoO_3$ nanosheets were favourable for the activation of N_2 and the formation of $^*N_2H$ (Fig. 4f). The experiments confirm that the effective NH_3 yield of Li$xMoO_3$ nanosheets is 3.48 μg cm^{-2} h^{-1}, 9 times that of MoO_3 nanosheets. The LDH systems with an abundance of surface oxygen vacancies or coordinatively unsaturated metal cations in ammonia synthesis were popular in N_2 reduction. Zhang *et al.* demonstrated a simple pretreatment of ZnCr-LDH,

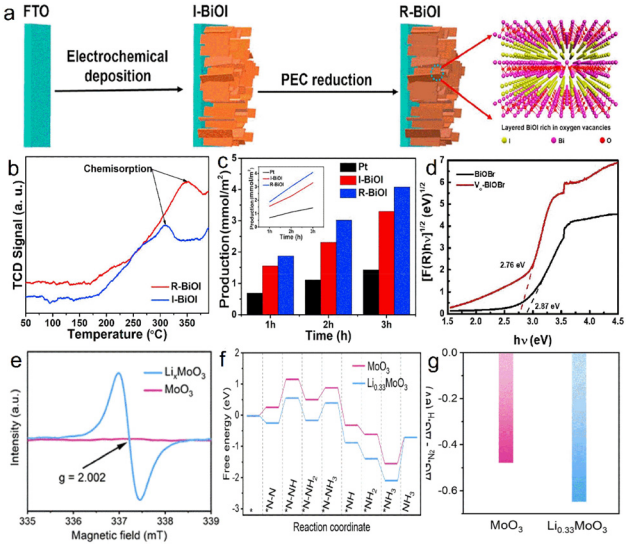

Fig. 4 (a) Schematic diagram of the synthesis process, of the I-BiOI/R-BiOI, (b) N_2-TPD profiles of the I-BiOI/R-BiOI, (c) production rate of ammonia,[24] Copyright 2019, Elsevier. (d) the bandgap of O_{VS}-BiOBr and BiOBr,[27] Copyright 2022, Elsevier. (e) EPR of MoO_3 and Li_xMoO_3, (f) free energy on oxygen vacancies (O_{VS}) of MoO_3 (010) and $Li_{0.33}MoO_3$ (010), (g) Gibbs free energy difference between $^*N_2$ and $^*H$ over MoO_3 (010) and $Li_{0.33}MoO_3$ (010).[64] Copyright 2022, Elsevier.

ZnAl-LDH, and NiAl-LDH nanosheets with aqueous NaOH, thus enhancing the concentration of oxygen vacancies to significantly improve photocatalytic activity for N_2 reduction to NH_3.[67]

Nitrogen vacancies (N_{vs}) exhibit enhanced performance for PEC N_2 reduction. Li *et al.* used 3-amino-1,2,4-triazole treated with NaOH as a precursor to prepare g-C_3N_5 with N_{vs},[68] and the N_{vs} realized charge separation by accepting electrons of g-C_3N_5. BiOBr/g-C_3N_5 heterostructures with N_{vs} are synthesized to realize the double-electron transfer mechanism (DETM). The DETM delays the recombination of carriers to ensure high-quality electrons, which is manifested through increased ammonia yield (BiOBr: 2.5 μg mg^{-1} h^{-1}; N_{vs}-g-C_3N_5: 14.8 μg mg^{-1} h^{-1}, N_{vs}-g-C_3N_5/BiOBr: 29.4 μg mg^{-1} h^{-1}).

3.2 Heteroatom doping

Metal/non-metal ion doping could adjust the electronic structure, redistribute the electron density, and construct surface defects.[69,70] The unoccupied orbitals of the TMs capture lone pair electrons of N_2 molecules due to matched orbital energy and symmetry, while the occupied d orbitals donate electrons in reverse to the anti-bonding orbitals of the N_2 molecule. Therefore, the strong triple bond of N_2 is weakened when the TM–N σ-bond is formed, thus promoting the activation of N_2. The most studied metal doping for photocatalytic nitrogen fixation is an iron ion with abundant unfilled 3d orbitals, variable valence and considerable cost. Schrauzer *et al.* improved the nitrogen-fixing activity of TiO_2 by doping Fe, Co, Mo or Cr, and found that 2%Fe-doped TiO_2 exhibited the best performance in photocatalytic NH_3 synthesis.[71] Vu *et al.* synthesized Fe-$W_{18}O_{49}$ nanorods with Au modification by two-step approach, in which the Fe existed in the form of Fe^{3+}/Fe^{2+}(Fig. 5a).[21] Fe-$W_{18}O_{49}$ enhanced light absorption ability and improved the separation capacity of electron–hole pairs, and achieved a high yield of NH_3 (9.82 μg h^{-1} cm^{-1}) under PEC conditions.

The doping of non-metallic atoms (such as B, P, N, *etc.*) is used to increase the VB position and reduce the bandgap through orbital hybridization or defect engineering.[73] Furthermore, non-metallic doping avoids the formation of recombination centers in N_2 reduction.[74,75] Xu *et al.* synthesized B-doped Bi from layered BiOBr nanosheets with sodium borohydride ($NaBH_4$) as a reductant,[72] and the injection of B atoms enhanced the polarization of Bi (012), and Bi provided electrons to the neighbouring B atoms, resulting in the change of the Bi oxidation state and surface geometry (Fig. 5c). The Bi surface with a high curvature promoted N_2 adsorption, and the accumulation of electrons on Bi facilitated the entry of electrons into the anti-bonding orbital of $^*NNH$, thus promoting the elongation of the N–N bond of $^*NNH$. The energy barrier of the potential-determining step was reduced to 2.00 eV, showing that B doping had a positive role in N_2 reduction (Fig. 5d). The B-doped Bi showed excellent PEC N_2 reduction performance (NH_3 yield: 29.2 mg $g_{cat.}^{-1}$ h^{-1}), far exceeding that of bismuth (10.6 mg $g_{cat.}^{-1}$ h^{-1}).

As a burgeoning class of two-dimensional materials, graphene is sought in the field of photocatalysis and electrocatalysis. Nitrogen doping can regulate the optical bandgap of graphene to endow favourable optical and electrical features through expanded π electron delocalization.[76] The introduction of nitrogen affects both the crystal structure and electronic structure of graphene, in addition, the polarity, electronic donor property, conductivity and chemical stability of graphene can be improved.[77,78] Nitrogen doping into carbon supporter generates regulated charge density, resulting in

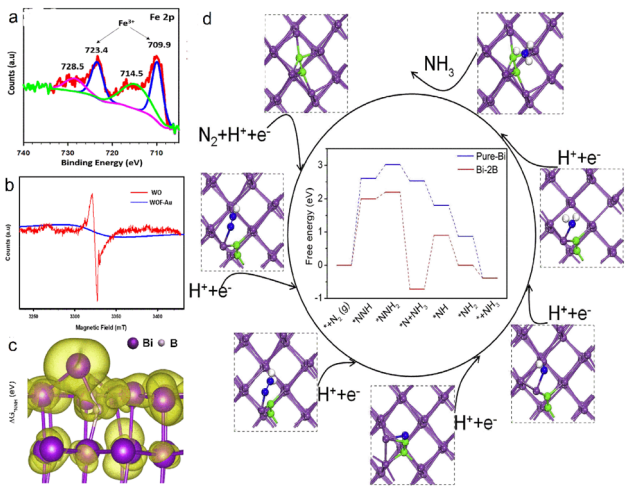

Fig. 5 (a) Fe 2p XPS of WOF-Au, (b) EPR of WO and WOF-Au,[21] Copyright 2020, American Chemical Society. (c) Partial charge density of the Bi-2B (012) facet, (d) N_2 reduction progress on Bi-2B (012).[72] Copyright 2020, Elsevier.

complex reactions related to the multi-proton and electron transfer in N_2 reduction. Meanwhile, studies have shown that the graphene lattice that is rich in nitrogen dopants contributes to the formation of n-type semiconductors.[79] Generally, nitrogen doped reduced graphene oxide (RGO) shows potential for p–n heterojunction construction, which is conducive to the formation of an electric field. Paramanik *et al.* constructed the composite of $CoTiO_3$ and N-RGO, where an electron is confined in the atomic layer when N-RGO grows on the surface of $CoTiO_3$. In addition, N-RGO/$CoTiO_3$ achieves a shorter diffusion distance of electrons, rapid charge transfer and small interface resistance.[80] In addition, the synergistic interaction between the rod-like structure of $CoTiO_3$ and the rough surface of N-RGO contributes to the overall improvement of the catalytic performance. The optimized 1N-RGO/$CoTiO_3$ has a quenching rate of 54.89% for photogenerated carriers, and possesses an electron lifetime of 3.0 ms. The photocatalytic and PEC activities are more than 1.7 $mmol^{-1}$ h^{-1} and 16 μg cm^{-1} h^{-1}, respectively.

Although nonmetallic doped catalysts have improved performance, the mechanism and stability still need to be further explored in view of the fact that the introduced elements may become the quenching sites of electrons and holes,[62] so it is indispensable to study the stabilization strategy for doping non-metallic elements.

3.3 Frustrated Lewis pairs (FLPs)

Metal-free catalytic ammonia synthesis with high selectivity and ideal yield faces challenges until the breakthrough of N_2 activation based on the frustrated Lewis pairs (FLPs) in 2018.[81] FLPs with an electrophilic acid and nucleophilic base are favorable for the breaking of N≡N through the electron transfer between the unoccupied orbitals of electrophilic acid and the nonbonding orbitals of nucleophilic base (Fig. 6a). Stephan *et al.* reported the space blockage in inhibiting the capture of N_2 in the synthesis of $Ph_2CN_2B(C_6F_5)_3$ with carbene, N_2 and borane as reactants.[82] Dai *et al.* presented boron carbon nitride (BCN) with the abundant unsaturated B (Lewis acid sites) and N atoms (base sites), and the results showed that FLPs adsorb N_2 molecules to form six membered ring intermediates, which reduces the energy of N≡N breaking.[83] Chen *et al.* proposed an alternative strategy based on FLP catalysts to stabilize N_2H^* intermediates, that is, substituting two-dimensional black phosphorus co-doped with TMs and boron atoms for FLPs.[84] Zhu *et al.* designed a variety of FLPs that have the ability to activate N_2, and exhibit low ΔG values of −37.5 to −51.0 kcal mol^{-1} (Fig. 6e).[81]

3.4 Heterojunction construction

Different from the inherent band structure of single-phase catalysts, heterojunction materials have the advantages of regulating the threshold of light absorption, accelerating the separation of carriers by changing the band structure, and passivating the recombination of electrons and holes. A typical heterojunction is an interface formed through the contact of two different semiconductors, which is mainly divided into types I, II and III (Fig. 7a–c). In type I, the VB and the CB of one semiconductor are more negative than those of another semiconductor, and there is no photocatalytic activity because the carriers cannot be effectively separated under photoexcitation. In type III heterojunction, the band positions of one semiconductor are all above the band positions of another semiconductor, and the formed interface has almost no catalytic activity in type III. For type II, the band positions are staggered between the two semiconductors, thus forming an upward or downward bending of the band,[89] which causes the charge carriers to migrate in the opposite direction, thus prolonging the life of electrons and holes and improving the redox ability. Although effective charge separation is accomplished in con-

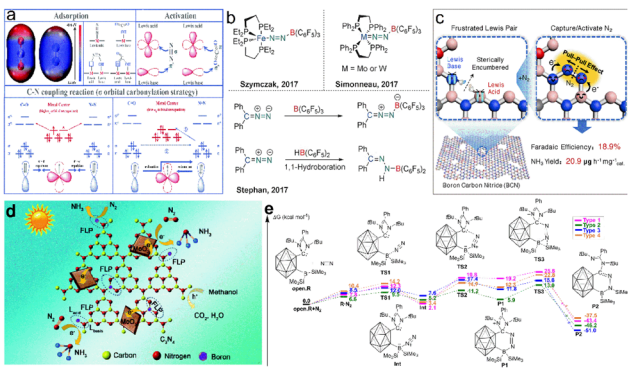

Fig. 6 (a) Illustration of artificial frustrated Lewis pairs to adsorb and activate N_2, C–N coupling reaction,[85] Copyright 2021, the Royal Society of Chemistry. (b) Lewis acidic boranes for N–N activation,[86] Copyright 2017, Wiley-VCH. (c) Schematic illustration of BCN for electrochemical nitrogen reduction,[83] Copyright 2022, Wiley-VCH. (d) Mechanism of over 10B/10Mo–C_3N_4 in the photocatalytic N_2 fixation strategy,[87] Copyright 2020, the Royal Society of Chemistry. (e) Gibbs energy over carborane-based FLPs for N_2 reduction.[81] Copyright 2022, American Chemical Society.

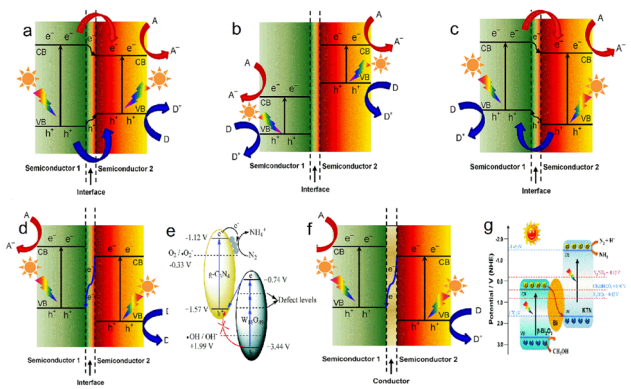

Fig. 7 Band structure of (a) type I, (b) type II, (c) type III, and (d) Z-scheme heterojunction in semiconductor–semiconductor and for example, (e) g-C_3N_4/$W_{18}O_{49}$,[33] Copyright 2017, the Royal Society of Chemistry. (f) Z-scheme in the semiconductor–electron mediator–semiconductor. A: electron acceptor, D: electron donor; and for example, (g) Bi-Bi_2O_3/$KTa_{0.5}Nb_{0.5}O_3$.[88] Copyright 2022, the Royal Society of Chemistry.

structed type II systems, the main disadvantage is the lower oxidation and poorer reduction capabilities.[90] The Z-scheme heterojunctions achieve rapidly separated carriers and strong redox ability, which can be attributed to the recombination of holes on the VB for one semiconductor and electrons on the CB for another semiconductor (Fig. 7d and e). The Z-scheme heterojunctions are divided into semiconductor–semiconductor (that is the S-scheme) and semiconductor–mediator–semiconductor depending on whether there is an electronic mediator between two semiconductors. Researchers have focused on the construction of different heterojunction nanocomposites,[91] aiming to boost the utilization of ultraviolet light or near-infrared light and to promote carrier separation for PEC nitrogen fixation.

Owing to the controllable chemical environment, metal–organic frameworks (MOFs) are used in the preparation of heterostructures as photoelectrodes.[92,93] Liu *et al.* used the *in situ* chemical etching strategy to form Cu-MOFs on the Cu_2O surface with an organic ligand (H_3BTC), and the Cu-MOF amount can be determined by etching time (Fig. 8a).[94] The establishment of the Cu-MOF/Cu_2O heterostructure improves the carrier density and charge separation efficiency (Fig. 8b). Meanwhile, the NH_3 yield of Cu-MOF/Cu_2O is increased to 7.2 mmol m^{-2} h^{-1} due to unsaturated Cu(II) sites, which is 5 times that of Cu_2O (3.7 mmol m^{-2} h^{-1}) and 3.9 times that of Cu-MOFs (1.9 mmol m^{-2} h^{-1}). Phthalocyanine copper is used for ammonia synthesis due to strong photoresponsiveness. However, the surface of phthalocyanine copper lacks an active site and does not have the desired surface reaction kinetics. Li *et al.* prepared a phthalocyanine copper/CeO_2 heterostructure by the chemical deposition method, and CeO_2 is coated on the phthalocyanine copper surface.[95] UV-Vis absorption and electrochemical measurement make it clear that the phthalocyanine copper/CeO_2 heterostructure has a wide absorption range and a high electrochemical activity area. The PEC N_2 reduction performance reaches the best with an NH_3 yield of 1.16 μmol h^{-1} cm^{-2}.

The C atom inserted into the Mo lattice shows a narrow metal band and exhibits similar Fermi level densities to noble metals, so Mo_2C is expected to perform well in catalysis.[98] However, Mo_2C is a matrix with poor electrical conductivity,[99] so it is necessary to consider the optimization of carrier migration for PEC N_2 reduction. Li *et al.* took graphite as a unit of the core–shell heterostructure, and wrapped it on the Mo_2C cluster surface based on *in situ* hydrothermal and calcination treatment, and effectively broke through the limitation of Mo_2C conductivity.[100] The graphitized carbon can accelerate electron transfer, which is conducive to the activation of N_2, with an NH_3 yield of 6.6 μg h^{-1} mg^{-1}. In addition, $MoSe_2$ and the two-dimensional material g-C_3N_4 are assembled to form heterojunctions. Mushtaq *et al.* synthesized layered flower-like $MoSe_2$-g-C_3N_4,[26] and the Mo–N bond between $MoSe_2$ and g-C_3N_4 enhances the internal conductivity of $MoSe_2$. The absorption capacity of $MoSe_2$-g-C_3N_4 is enhanced (Fig. 8c), and the $MoSe_2$-g-C_3N_4 hybrid shows efficient PEC N_2 reduction performance with an FE of 28.91% and a yield of 7.72 mmol h^{-1} cm^{-2}, respectively (Fig. 8d). The associative distal pathway and Gibbs free energy on $MoSe_2$@g-C_3N_4 heterojunctions are shown in Fig. 8e and f. The results show that N_2 is well adsorbed and activated on the $MoSe_2$-g-C_3N_4 (7 wt%) hybrid surface.

WO_3 is widely used as a photo/electrocatalyst due to its tunable composition, favourable stability and abundant availability. Guo *et al.* simulated a heterojunction constructed by WO_3 and metal dichalcogenides (MoS_2, WSe_2), and proved that heterojunctions are stable in thermodynamics through calculation (Fig. 8g). In particular, optimized WO_3-MoS_2 has the lowest onset potential (0.25 V),[96] and its catalytic performance is enhanced by re-positioning the d-band center that is precisely controlled to a higher energy level. Furthermore, in order to improve the N_2 reduction activity, porous skeleton structures are used in heterojunction construction engineering. Multiple scattering and absorption of light in the porous structure are conducive to the efficient capture of sunlight.[101–103] Porous CdS was obtained by growing CdS on Mo doped WO_3 hollow microspheres based on the hydrothermal method. The Mo-WO_3@CdS heterostructure[104] achieved a FE of 36.72% and an NH_3 yield of 38.99 μg h^{-1} mg^{-1}. The DFT analysis suggests that Mo–W is the catalytic center of N_2 reduction, and CdS promotes the provision of electrons, thus accelerating PEC N_2 hydrogenation. Meanwhile, the development of porous structures provides the basis for functionalized heterogeneous structures. The Au modified porous polytetrafluoroethylene (PTFE) skeleton dispersed on a silicon-based electrode was synthesized. The

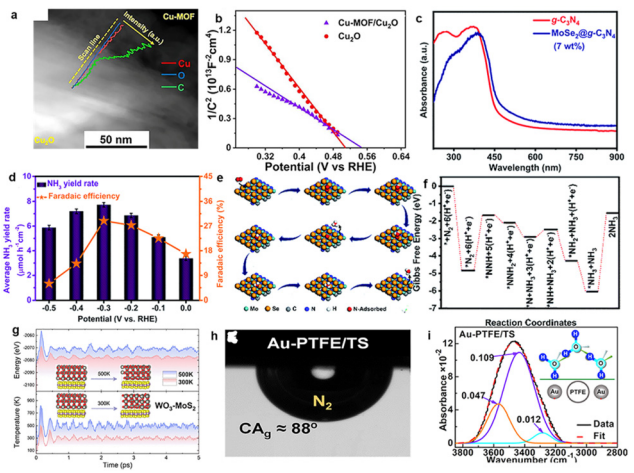

Fig. 8 (a) TEM images and EDS spectra of Cu-MOF/Cu_2O, (b) Mott–Schottky plot (frequency: 800 Hz),[94] Copyright 2021, Elsevier. (c) optical bandgap energy of g-C_3N_4 and $MoSe_2$@g-C_3N_4, (d) equivalent NH_3 yield and FE at different potentials on $MoSe_2$@g-C_3N_4 heterojunctions, (e) associative distal pathway for PEC N_2 reduction, (f) Gibbs free energy on $MoSe_2$@g-C_3N_4 heterojunctions,[26] Copyright 2020, the Royal Society of Chemistry. (g) Fluctuation of temperature and energy against the time of WO_3-MoS_2 at 300 K and 500 K,[96] Copyright 2022, American Chemical Society. (h) The image of an underwater N_2 bubble on the Au-PTFE/TS surface, (i) original (black line) and deconvoluted (red line) spectra of interfacial water at the Au-PTFE/TS surface.[97] Copyright 2019, Elsevier.

silicon and the porous PTFE skeleton were used as the light absorber and gas diffusion channels, respectively, while Au was used as the reaction site.[97] Attenuated total reflection and caption-bubble measurements demonstrated that the porous framework of Teflon and Au created a gas-hydrophilic structure, which promoted N_2 enrichment and controlled proton activity in aqueous solution (Fig. 8h and i). The optimal ammonia production rate of the photocathode is about 18.9 μg cm^{-2} h^{-1}, and the FE is 37.8% at −0.2 V *vs.* RHE. The LDH plays a key role in the fields of photocatalysis/electrocatalysis and energy conversion due to easily controllable composition and abundance of surface oxygen vacancies or coordinatively.[105] Yan *et al.* constructed a CoVP@NiFeV-LDH heterojunction that has shown excellent electrocatalytic performance in the N_2 reduction reaction. The new three-dimensional hollow hierarchical structure provides abundant active sites for nitrogen adsorption and reduction to NH_3.[106]

3.5 Cocatalyst loading

Noble metal catalysts have the advantages of high catalytic activity, stability and selectivity. For effective utilization of noble metals, it is necessary to load them onto the host matrix. For example, black silicon serves as a carrier, and it can also enhance light absorption and suppress reflection.[107,108] Ali *et al.* used plasma-enhanced black silicon decorated with Au nanoparticles (NPs) to achieve photoelectrically driven nitrogen conversion (Fig. 9a).[22] When black silicon is replaced by unetched silicon, NH_3 production is 11% of that generated by Au/black Si/Cr. Black silicon provides a large surface area for Au loading. Au-coated black silicon has a higher ammonia yield (more than 13 mg m^{-2} h^{-1}) than black silicon. Wang *et al.* realized the PEC process of converting nitrogen into ammonia, when black silicon was used to enhance light absorption, and silver was used as an active site with a FE of 55.05% at −0.1 V (*vs.* RHE).[25]

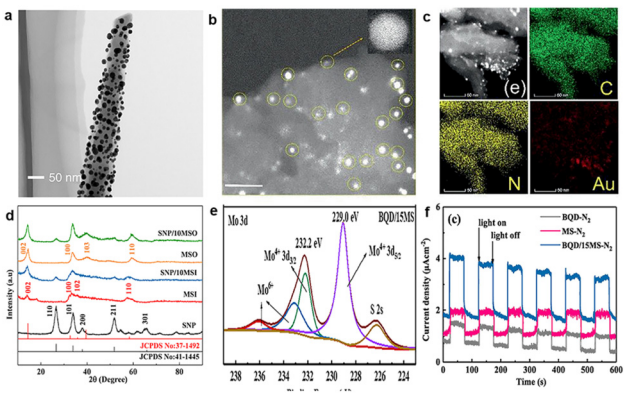

Fig. 9 (a) Corresponding TEM images of Au-coated silicon nanowires,[22] Copyright 2016, Nature Publishing Group. (b) TEM images of Au/g-C_3N_4, (c) mapping of N, C, and Au,[109] Copyright 2021, Wiley-VCH. (d) XRD patterns of SnO_2/10MoS_2, SnO_2/10MoS_2 (silicomolybdic acid is not a precursor), MoS_2 (silicomolybdic acid is not a precursor) and SnO_2,[110] Copyright 2022, Elsevier. (e) The XPS spectra of Bi_2S_3 QDs/15MoS_2, (f) photocurrent with a light on–off cycle.[111] Copyright 2022, Elsevier.

Porous structures are also excellent to disperse and stabilize metal NPs. Peramaiah *et al.* deposited Au NPs on porous g-C_3N_4 with N defects, and then coated it on the n^+np^+-Si photocathode surface (Fig. 9b and c).[109] Silicon plays the roles of light collection and electrical management, Au is the active center to promote the conversion of N_2 to NH_3, and porous g-C_3N_4 with N-defects provides more N_2 adsorption sites. Each N atom is alternately associated with the first and second hydrogenation; then, the third hydrogen is added to destroy the N–N bond; finally, the distal N atom is reduced thoroughly with the release of the first NH_3 molecule. Au/g-C_3N_4 exhibits excellent PEC N_2 reduction performance with a FE of up to 61.8% and an NH_3 yield of 13.8% μg h^{-1} cm^{-2}. MoS_2 is an excellent carrier due to its well-dispersed layered structure, high conductivity and large specific surface area. Ye *et al.* dispersed TiO_2 NPs on MoS_2 nanosheets by the hydrothermal method, and the addition of MoS_2 leads to a smaller bandgap (2.98 eV) than that of TiO_2, and expedites the separation of electrons and holes.[112] Enhanced charge transfer maintains higher photoelectric voltage and slower decay behaviour. The results show that the NH_3 yield and FE are 1.42×10^{-6} mol h^{-1} cm^{-2} and 65.52%, respectively, for MoS_2@TiO_2. Hydrophilic SnO_2 is uniformly dispersed on the surface of hydrophobic MoS_2, which leads to a change in the growth direction of MoS_2, so as to induce the growth of the (002) crystal plane. The improved transfer and separation of carriers are attributed to the strong interaction between SnO_2 and MoS_2, with an NH_3 yield of 19.6 at −0.3 V μg h^{-1} mg^{-1} and a FE of 40.34%, much higher than those of individual SnO_2 and MoS_2 (Fig. 9d).

Quantum dots (QDs) possess superior properties that play important roles in N_2 reduction,[113] such as small size, strong photostability, multiple excitation, exposed sites and electronic peculiarity. For example, Bi_2S_3 QDs have a high absorption coefficient and narrow bandgap.[114] Gao *et al.* grew Bi_2S_3 QDs on MoS_2 through hydrothermal and solvothermal processes for photocatalytic reduction of N_2 to NH_3.[111] Bi_2S_3 QDs were dispersed on the MoS_2 surface, and the agglomeration of Bi_2S_3 QDs can be inhibited. The shift of binding energy indicates that there is an interaction between Bi_2S_3 QD and MoS_2 (Fig. 9e), thus leading to electron transfer from Bi_2S_3 to MoS_2 and accelerating the carrier separation (Fig. 9f). The FE of the Bi_2S_3 QD/15MoS_2 photocathode reaches 33%, and the NH_3 yield is 19 μg h^{-1} mg^{-1}. Carbon quantum dots (CQDs) are narrow-gap semiconductor materials, and Hu *et al.* synthesized CQD-modified hydrogenated mesoporous $SrTiO_3$ (CQDs/STO) based on the small size and good conductivity.[115] The ammonia yield of CQDs/STO is 143 μmol g^{-1} h^{-1} and is 7 times that of STO without a sacrificial agent. Furthermore, heterogeneous CQD/STO with a defective STO (200) surface can promote catalytic N_2 conversion.

3.6 Other advanced catalysts and strategies for nitrogen fixation

Single atomic alloy catalysts have broad application prospects in electro-catalytic nitrogen reduction because of the highly exposed active sites. However, there are limited comprehensive

experiments and theoretical research on the conversion of N_2 to nitrogen-containing molecules. Chuk *et al.* reported that the yield of NH_3 in the nitrogen reduction reaction was 111.9 μg h^{-1} mg^{-1} using single atom PdFe alloy.[116] In addition, compared with the pristine Ru, the use of Ru–Cu alloy showed that the addition of Cu improved the FE of NH_3 (31%) through enhanced N_2 adsorption and a reduced H barrier.[117] Li-mediated N_2 reduction is flexible in the electrocatalytic approach, which has practical significance for realizing the nitrogen cycle; however, the yield and FE are not optimistic. Du *et al.* studied the properties of the interface generated by the imide-based Li salt electrolytes. The constructed interface can provide a substantial NH_3 yield of 150 ± 20 nmol s^{-1} cm^{-2}, and a FE of up to 100%.[118] In addition, this group has realized the ammonia synthesis by the phosphonium cation and isopropanol.[119] Therefore, the development of non-metallic materials with high nitrogen fixation efficiency is of great potential. Recently, both experiments and theoretical calculations have suggested that traditional semiconductor materials are promising photoelectrocatalysts for N_2 reduction under ambient conditions, as listed in Table 1.

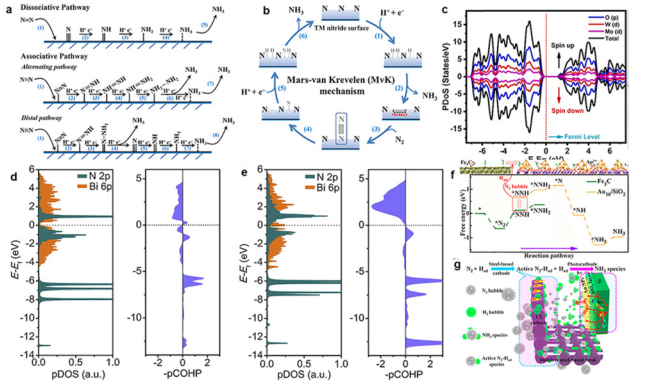

Fig. 10 (a) Dissociative, distal and alternating pathways for N_2 reduction, (b) MvK mechanism on the TM nitride surface,[132] (c) atom projected density of states (PDOS) of Mo-WO_3,[104] Copyright 2022, Elsevier. (d and e) PDOS and projected crystal orbital Hamilton populations of the N atoms (*NNH) on Bi (012) and (e) Bi-2B (012),[72] Copyright 2021, Elsevier. (f) Free energy and optimized geometric structure of distal mechanisms on the Fe_3C sites and Au^{1+} sites of the Au/SiO_2/Si photocathode, (g) schematic representation of the catalytic and enhanced mechanism of the PEC NRR on the Au/SiO_2/Si photocathode.[133] Copyright 2021, American Chemical Society.

4. Mechanism of PEC N_2 reduction for ammonia synthesis

It is generally believed that PEC N_2 reduction on a heterogeneous catalyst surface undergoes two mechanisms, namely the associative reaction and dissociative reaction (Fig. 10a).[23] For dissociation, the triple bond of N_2 is cracked before hydrogenation, and two separate N atoms are reduced to form NH_3 independently through hydrogenation steps, which is similar to the H–B process that requires more energy. In the association pathway, two nitrogen atom centers are combined together when the N_2 molecule is hydrogenated, and NH_3 is released with the breaking of the N≡N bond. The hydrogenation in the association mechanism can take place in two possible ways, namely distal and alternative pathways. When N_2 appears in the mode of terminal coordination, hydrogenation is inclined to occur on the nitrogen far from the catalysts, thus leading to the generation of NH_3 molecules, and leaving the metal nitrogen unit to react with H^+ to generate another NH_3 molecule. The alternative route requires that two nitrogen centers alternate between two N atoms on the catalytic surface. After the first NH_3 is removed, the second NH_3 will be released immediately. Our group has reported the possible route (distal pathway) of NH_3 synthesis on the $MoSe_2$-g-C_3N_4 surface based on the Gibbs free energy,[26] that is, the adsorbed N_2 is hydrogenated by H^+ adsorption and electron transfer to form an N_2H^* group at the Mo site. And then $H^+ + e^-$ reacts with N to form N_2H^*. The adsorption of H^+ on the pre-hydrogenated N site of $N_2H_2^*$ yields an NH_3 molecule, leaving the remaining N at the Mo atom. After that, another three H^+ ions are coupled to the electron, hydrogenating the remaining N^* molecule to give a second NH_3.

Researchers proposed a new reaction mechanism in recent years, namely Mars–van-Krevelen (MvK), based on transition

Table 1 The catalytic performance of PEC N_2 reduction to NH_3 over various catalysts

Catalyst	Irradiation source	Bias [V]	Rate of NH_3	Ref.
$BiVO_4$/PANI	300 W Xe lamp	−0.1 V *vs.* RHE	0.055 μmol cm^{-2} h^{-1}	52
BiOI	100 mW cm^{-2}	+0.4 V *vs.* RHE	0.140 μmol cm^{-2} h^{-1}	24
CQDs/$SrTiO_3$	300 W Xe lamp	−0.3 V *vs.* RHE	1.915 μmol cm^{-2} h^{-1}	115
Cu_2O	300 W Xe lamp	+0.4 V *vs.* RHE	0.423 μmol cm^{-2} h^{-1}	49
PANI-ASSM/CdS-Co_3S_4	40 W LED	−0.75 V *vs.* RHE	12.33 μmol cm^{-2} h^{-1}	120
Vo-BiOBr/TiO_2	300 W Xe lamp	−0.2 V *vs.* RHE	1.475 μmol cm^{-2} h^{-1}	27
Cu-MOF/Cu_2O	300 W Xe lamp	+0.5 V *vs.* RHE	0.716 μmol cm^{-2} h^{-1}	94
$MoSe_2$@g-C_3N_4	150 W Xe lamp	−0.3 V *vs.* RHE	7.72 μmol cm^{-2} h^{-1}	26
Fe-doped $W_{18}O_{49}$	simulated solar light	−0.65 V *vs.* Ag/AgCl,	0.577 μmol cm^{-2} h^{-1}	21
SnO_2/MoS_2	300 W Xe lamp	−0.3 V *vs.* RHE	19.6 μg h^{-1} $mg_{cat.}^{-1}$	110
B-doped Bi nanorolls	300 W Xe lamp	+0.48 V *vs.* RHE	29.2 mg h^{-1} $g_{cat.}^{-1}$	72
Mo-doped WO_3@CdS	300 W Xe lamp	−0.3 V *vs.* RHE	38.99 μg h^{-1} $mg_{cat.}^{-1}$	101
Mo_2C/C	100 mW cm^{-2}	+0.2 V *vs.* Ag/AgCl	6.6 μg h^{-1} $mg_{cat.}^{-1}$	121

metal nitrides (TMNs: V–N, Zr–N, Nb–N) as shown in Fig. 10.[122] The lattice N atoms of TMNs are hydrogenated to obtain NH_3 by lattice nitrogen reduction, followed by the regeneration of lattice nitrogen. Importantly, N_2 activation on TMNs requires a smaller overpotential for the MvK mechanism, which is more conducive to the formation of NH_3 than association and dissociation reactions.

DFT studies are used for energy assessment and catalyst design on the basis of experimental results, including the calculations of adsorption energy, Gibbs free energy,[75,123,124] the density of states analysis, the Bader charge analysis, and the crystal orbital Hamilton population analysis. In addition, advanced *in situ* monitoring technologies are meaningful for verifying the reaction mechanisms, dynamics of molecular catalyst interactions, and revealing the structure of intermediates, especially for *in situ* observation of catalytic reaction intermediates under practical operation, such as synchrotron radiation, X-ray diffraction (XRD), X-ray photoelectron spectroscopy (XPS), scanning tunnelling microscopy (STM), X-ray absorption spectroscopy (XAS), diffuse reflectance infrared Fourier transform spectroscopy (DRIFTS) and surface-enhanced infrared absorption spectroscopy (SEIRAS).[125–128] Yang *et al.* used *in situ* XPS and *in situ* XAS to reveal that $VN_{0.7}O_{0.45}$ was the active site rather than VN, and they monitored that the catalyst underwent passivation due to a change in $VN_{0.7}O_{0.45}$ to form VN.[129] According to *in situ* SEIRAS, the possible nitrogen reduction pathway on the Ru surface in acidic solution was deduced.[130] Feng *et al.* observed that adsorbed H_2O molecules were located at the O_{vs} site based on *operando* STM equipment, which accelerated the electrocatalytic HER process, and provided a rich route for revealing the kinetic process of nitrogen fixation.[131] Various *in situ* characterization techniques can be used not only independently, but also in combination to obtain accurate and multi-dimensional research results. In the future, *in situ* characterization technology will make a breakthrough in cost and universality, which further deepens our understanding of catalytic mechanisms.

The selectivity of NH_3 from N_2 and H_2O is challenging against the HER (and/or N_2H_4), and numerous computational simulations and experimental attempts have been conducted to elucidate the essence of selectivity. Singh *et al.* provided some guidance that the selectivity between NH_3 and H_2 can be determined through a competition between the binding energies of N and H. They found that the generation rate of ammonia is of zero-order at electron and proton concentrations, while the rate of H_2 is of first-order at a potential more negative than Us (Us refers to the potential to favourable H adsorption).[134] And the strategies of proton/electron availability have been proposed due to the significant impact of the proton concentration on HER performance, so employing an aprotic solvent,[135] blanketing the catalyst with a hydrophobic protection layer,[136] and designing photoelectrocatalysts are several potential solutions to selectively block the proton transfer to the catalyst surface, thus hindering H_2 evolution. Increased loadings of H^+ and e^- equivalents can directly translate to greater N_2H_4 yields, and the powerful reductant KC_8 and strong Brønsted acid can deliver H^+/e^- equivalents for the necessary proton-coupled electron transfer to improve the selectivity of N_2H_4.[137] In addition, regulating the adsorption strength of N and H towards catalytic sites can alter the selectivity of NH_3. It is reported that the adsorption energy of H on Ru is smaller than that on N, which indicates that N atoms are preferably adsorbed on H atoms, thus obtaining higher NH_3 selectivity.[138]

5. Detection and quantification of nitrogen sources for ammonia

The accurate quantification of ammonia is restricted by many factors, such as trace NH_3 yield intrinsically, ammonia pollution from the environment, tedious ammonia separation from electrolytes, solution pH, and interferants. Serious concerns exist on a reliable quantitative method of ammonia concentration for N_2 reduction, and we should maintain a rigorous scientific attitude and strive to accurately quantify NH_3 based on different catalytic systems (Fig. 11). Currently, spectrophotometry and ion chromatography are common methods with the advantage of simplicity. In addition, the use of ion-selective electrodes (ISEs) and colorimetric NH_3 assay kits, and nuclear magnetic resonance (NMR) methods can significantly improve the sensitivity, however, the experimental cost is increased to a certain extent.

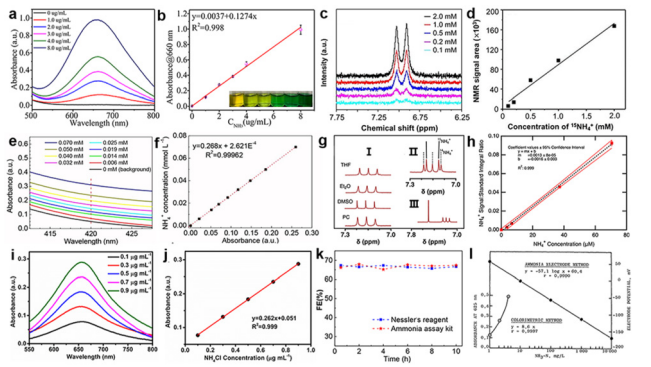

Fig. 11 Calibration curves for NH_3 quantification. (a) the UV-Vis absorption, (b) the corresponding calibration curve for the indophenol blue method,[147] Copyright 2019, Wiley-VCH. (c) ^1H NMR spectra of $^{15}NH_4^+$ standard solutions (0.1–2.0 mM), (d) the corresponding calibration curve for the NMR method,[49] Copyright 2020, American Chemical Society. (e) UV-Vis of standard solutions, and (f) the corresponding calibration curve with Nessler's reagent,[145] Copyright 2019, Nature Publishing Group. (g) (I) ^1H NMR of NH_4^+ in 100 μM NH_4^+ in various solvents, (II) NMR spectra of a mixture of $^{14}NH_4^+$+$^{15}NH_4^+$, (III) NMR of the $LiClO_4$/THF electrolyte after N_2 reduction, (h) calibration curve to determine the NH_4^+ concentration,[144] Copyright 2019, American Chemical Society. (i) UV-Vis absorption spectra and (j) the calibration curve using salicylic acid,[104] Copyright 2022, Elsevier. (k) FE of ammonia measured using Nessler's reagent or an enzymatic ammonia assay kit,[145] Copyright 2019, Nature Publishing Group. (l) The ion-selective electrode method.[148] Copyright 1969, Springer Nature.

The universal chemical chromogenic approaches are indophenol blue (IB) and Nessler's reagent based on the calibration curve, and they all have limitations. The IB test is usually used under neutral and acidic conditions because the generated indophenol dye could react with other amine groups under alkaline conditions.[139] Sodium salicylate is more steady than IB because salicylate can prevent the generation of toxic substances.[140] Nessler's method has wide pH applicability, however, some sacrificial agents (alcohol, glucose) are oxidized to carbonyl easily, thus resulting in misleading results.[35] Ion chromatography has high sensitivity and reliable results, among which the distraction of pH and sacrificial agents are avoided through appropriate detection methods.[141,142] The ISE determines the concentration of ions in solution by a membrane potential based on the Nernst equation, which can be divided into the NH_4^+-selective electrode and the NH_3-selective electrode. The concentrated solution can further improve the accuracy of NH_3 detection when choosing an ISE.[143] The resonance signal obtained from ^1H can be qualitatively and quantitatively detected by NH_4^+.[144] Nielander *et al.* reported a frequency-selective pulse NMR method for measuring NH_3 concentration in electrolytes and quantified the common Berthelot method. The reliability of the results can be greatly improved by using various methods simultaneously to realize the quantitative determination of ammonia. Hao *et al.* used a colorimetric method with Nessler's reagent, an enzymatic NH_3 assay kit (Sigma-Aldrich), and NMR to quantify ammonia accurately;[145] they found that the FEs measured using Nessler's approach or the enzymatic ammonia assay kit are persuasive. Zhang *et al.* used Nessler's approach, ion chromatography and the indole phenol method to quantify NH_3, and the results showed that the three methods had good coordination at low concentrations (0–500 μg L^{-1}). However, Nessler's approach and ion chromatography are more suitable for the quantification of ammonia than the indole phenol method at high concentrations.[146]

In order to scale up the PEC ammonia synthesis technology, the most essential progress is to confirm the true role of the catalysts. The primary task of removing nitrogen pollution is to ensure that the feed gases and catalysts are not polluted by nitrogen containing substances, including nitrate, nitrite and other contaminants before the experiment. Considering serious ammonia pollution in the environment, the $^{15}N_2$ labeling experiment is necessary to provide direct evidence,[149] especially for N-containing catalyst systems.[123] However, many researchers often ignore the problem of $^{15}N_2$ pollution, so it is only used as a qualitative method. Therefore, we need to accurately present the nitrogen fixation performance of the catalysts from multiple views. In addition, the background experiment is another piece of evidence to assist in proving the role of catalysts. The development of a combined technology of ammonia synthesis and ammonia detection can avoid ammonia pollution and realize the *in-situ* detection and online quantification of ammonia.

6. Conclusion

The above achievements have proved that PEC N_2 reduction is a promising route to realize the N-cycle goal under environmental conditions, and multiple catalytic strategies are proposed to improve the yield and selectivity of NH_3. However, there are fundamental challenges as follows:

(I) Disclosure of the essence of photo-electrical synergy. The catalytic performance of PEC N_2 reduction is more excellent than that of individual photocatalysis or electrocatalysis; however, this collaborative technology causes obstacles to the mechanistic understanding and revelation of photogenic/electrical effects. Most studies show that light irradiation promotes the electrocatalytic process, and bias accelerates the separation of photogenerated carriers, and few works reveal the coexistence of photocatalytic and electrocatalytic processes.

(II) Reliable methods in consideration of NH_3 quantification and N-source determination. Although the spectral analysis is maneuverable, the accuracy usually is disturbed by pH, ionic strength and sacrificial agents. Therefore, it is necessary to combine it with other quantitative experiments, such as ion chromatography and NMR, to obtain accurate NH_3 concentrations. In addition, researchers judge the rationality of catalytic performance by testing the recommended benchmark catalyst.

(III) Rigorous mechanistic insights. The active sites, free energies and possible reaction paths are revealed on the basis of theoretical exploration. The available theoretical methods, catalyst model and computing power are the driving force behind accurate calculations.

(IV) Advanced *in situ* characterization. It is difficult to predict the reconstruction of the surface structure, including the change of valence states, the identification of reaction intermediates and active centers, and real-time monitoring of reaction processes. For example, *in situ* surface enhanced infrared absorption spectroscopy and high-resolution electron energy loss spectroscopy showed potential for understanding the N_2 reduction pathway due to its high sensitivity to the catalyst surface. In conclusion, reasonable catalysts are designed based on calculation and experiment, which will promote the rapid development of PEC N_2 reduction to a large extent under environmental conditions in the future. The advantages of PEC N_2 reduction are higher than those of individual photocatalysis or electrocatalysis. The correlation between PEC performance and the structures could be established at the molecular level to achieve industrial capabilities. In addition, strengthening durability testing is the key to proving the practicality at the industrial level. Finally, large-scale synthesis of catalysts should be considered.

Author contributions

Pengyan Li: methodology, investigation, and writing – original draft. Yumin Liu: supervision. Muhammad Asim Mushtaq: supervision. Dongpeng Yan: supervision and writing – review

& editing. The manuscript was written through contributions of all authors. All authors have given approval to the final version of the manuscript.

Conflicts of interest

There are no conflicts to declare.

Acknowledgements

This work was supported by the National Natural Science Foundation of China (Grant No. 22288201 and 22275021) and the Beijing Municipal Natural Science Foundation (Grant No. JQ20003).

References

1 S. Chen, D. Liu and T. Peng, Fundamentals and recent progress of photocatalytic nitrogen–fixation reaction over semiconductors, *Sol. RRL*, 2020, **5**, 2000487.
2 L. Wang, W. Wu, K. Liang and X. Yu, Advanced strategies for improving the photocatalytic nitrogen fixation performance: a short review, *Energy Fuels*, 2022, **36**, 11278–11291.
3 R. Shi, X. Zhang, G. I. N. Waterhouse, Y. Zhao and T. Zhang, The journey toward low temperature, low pressure catalytic nitrogen fixation, *Adv. Energy Mater.*, 2020, **10**, 2000659.
4 J. Lee, L. L. Tan and S. P. Chai, Heterojunction photocatalysts for artificial nitrogen fixation: fundamentals, latest advances and future perspectives, *Nanoscale*, 2021, **13**, 7011–7033.
5 Z. Zhao, H. Ren, D. Yang, Y. Han, J. Shi, K. An, Y. Chen, Y. Shi, W. Wang, J. Tan, X. Xin, Y. Zhang and Z. Jiang, Boosting nitrogen activation via bimetallic organic frameworks for photocatalytic ammonia synthesis, *ACS Catal.*, 2021, **11**, 9986–9995.
6 H. Liu, P. Wu, H. Li, Z. Chen, L. Wang, X. Zeng, Y. Zhu, Y. Jiang, X. Liao, B. S. Haynes, J. Ye, C. Stampfl and J. Huang, Unravelling the effects of layered supports on Ru nanoparticles for enhancing N_2 reduction in photocatalytic ammonia synthesis, *Appl. Catal., B*, 2019, **259**, 118026.
7 Y. Gao, S. Zhang, X. Sun, W. Zhao, H. Zhuo, G. Zhuang, S. Wang, Z. Yao, S. Deng, X. Zhong, Z. Wei and J.-G. Wang, Computational screening of O-functional MXenes for electrocatalytic ammonia synthesis, *Chin. J. Catal.*, 2022, **43**, 1860–1869.
8 P. Y. Li, L. Liu, W. An, H. Wang, H. X. Guo, Y. H. Liang and W. Q. Cui, Ultrathin porous g-C_3N_4 nanosheets modified with AuCu alloy nanoparticles and C–C coupling photothermal catalytic reduction of CO to ethanol, *Appl. Catal., B*, 2020, **266**, 118618.
9 X.-Y. Dao and W.-Y. Sun, Single- and mixed-metal–organic framework photocatalysts for carbon dioxide reduction, *Inorg. Chem. Front.*, 2021, **8**, 3178–3204.
10 M. Yang, C. H. Zhang, N. W. Li, D. Luan, L. Yu and X. W. D. Lou, Design and synthesis of hollow nanostructures for electrochemical water splitting, *Adv. Sci.*, 2022, **9**, e2105135.
11 Q. Liu, T. Xu, Y. Luo, Q. Kong, T. Li, S. Lu, A. A. Alshehri, K. A. Alzahrani and X. Sun, Recent advances in strategies for highly selective electrocatalytic N_2 reduction toward ambient NH_3 synthesis, *Curr. Opin. Electrochem.*, 2021, **29**, 100766.
12 W. Song, L. Yue, X. Fan, Y. Luo, B. Ying, S. Sun, D. Zheng, Q. Liu, M. S. Hamdy and X. Sun, Recent progress and strategies on the design of catalysts for electrochemical ammonia synthesis from nitrate reduction, *Inorg. Chem. Front.*, 2023, 3489–3514.
13 Q. Liu, L. Xie, J. Liang, Y. Ren, Y. Wang, L. Zhang, L. Yue, T. Li, Y. Luo, N. Li, B. Tang, Y. Liu, S. Gao, A. A. Alshehri, I. Shakir, P. O. Agboola, Q. Kong, Q. Wang, D. Ma and X. Sun, Ambient ammonia synthesis via electrochemical reduction of nitrate enabled by $NiCo_2O_4$ Nanowire Array, *Small*, 2022, **18**, e2106961.
14 J. Han, Z. Liu, Y. Ma, G. Cui, F. Xie, F. Wang, Y. Wu, S. Gao, Y. Xu and X. Sun, Ambient N_2 fixation to NH_3 at ambient conditions: Using Nb_2O_5 nanofiber as a high-performance electrocatalyst, *Nano Energy*, 2018, **52**, 264–270.
15 Z. Du, J. Liang, S. Li, Z. Xu, T. Li, Q. Liu, Y. Luo, F. Zhang, Y. Liu, Q. Kong, X. Shi, B. Tang, A. M. Asiri, B. Li and X. Sun, Alkylthiol surface engineering: an effective strategy toward enhanced electrocatalytic N_2-to-NH_3 fixation by a CoP nanoarray, *J. Mater. Chem. A*, 2021, **9**, 13861–13866.
16 D. Bao, Q. Zhang, F. L. Meng, H. X. Zhong, M. M. Shi, Y. Zhang, J. M. Yan, Q. Jiang and X. B. Zhang, Electrochemical reduction of N_2 under ambient conditions for artificial N_2 fixation and renewable energy storage using N_2/NH_3 cycle, *Adv. Mater.*, 2017, **29**, 1604799.
17 H. Ma, Z. Chen and Z. Wang, Electroreduction of nitrogen to ammonia on nanoporous gold, *Nanoscale*, 2021, **13**, 1717–1722.
18 Z. Y. Niu, L. Jiao, T. Zhang, X. M. Zhao, X. F. Wang, Z. Tan, L. Z. Liu, S. Chen and X. Z. Song, Boosting electrocatalytic ammonia synthesis of Bio-inspired porous Mo-doped hematite via nitrogen activation, *ACS Appl. Mater. Interfaces*, 2022, **14**, 55559–55567.
19 X. Xu, X. Liu, J. Zhao, D. Wu, Y. Du, T. Yan, N. Zhang, X. Ren and Q. Wei, Interface engineering of MoS_2@Fe$(OH)_3$ nanoarray heterostucture: Electrodeposition of MoS_2@Fe$(OH)_3$ as N_2 and H^+ channels for artificial NH_3 synthesis under mild conditions, *J. Colloid Interface Sci.*, 2022, **606**, 1374–1379.
20 X. Niu, A. Shi, D. Sun, S. Xiao, T. Zhang, Z. Zhou, X. A. Li and J. Wang, Photocatalytic ammonia synthesis: mechanistic insights into N_2 activation at oxygen vacancies under visible light excitation, *ACS Catal.*, 2021, **11**, 14058–14066.

21 M. H. Vu, C. C. Nguyen and T. O. Do, Synergistic effect of Fe doping and plasmonic Au nanoparticles on $W_{18}O_{49}$ nanorods for enhancing photoelectrochemical nitrogen reduction, *ACS Sustainable Chem. Eng.*, 2020, **8**, 12321–12330.

22 M. Ali, F. Zhou, K. Chen, C. Kotzur, C. Xiao, L. Bourgeois, X. Zhang and D. R. MacFarlane, Nanostructured photoelectrochemical solar cell for nitrogen reduction using plasmon-enhanced black silicon, *Nat. Commun.*, 2016, **7**, 11335.

23 H. Zheng, S. Zhang, X. Liu and A. P. O'Mullane, The application and improvement of TiO_2 (titanate) based nanomaterials for the photoelectrochemical conversion of CO_2 and N_2 into useful products, *Catal. Sci. Technol.*, 2021, **11**, 768–778.

24 Y. Bai, H. Bai, K. Qu, F. Wang, P. Guan, D. Xu, W. Fan and W. Shi, In-situ approach to fabricate BiOI photocathode with oxygen vacancies: understanding the N_2 reduced behavior in photoelectrochemical system, *Chem. Eng. J.*, 2019, **362**, 349–356.

25 B. Wang, L. Yao, G. Xu, X. Zhang, D. Wang, X. Shu, J. Lv and Y.-C. Wu, Highly efficient photoelectrochemical synthesis of ammonia using plasmon-enhanced black silicon under ambient conditions, *ACS Appl. Mater. Interfaces*, 2020, **12**, 20376–20382.

26 M. A. Mushtaq, M. Arif, X. Fang, G. Yasin, W. Ye, M. Basharat, B. Zhou, S. Yang, S. Ji and D. Yan, Photoelectrochemical reduction of N_2 to NH_3 under ambient conditions through hierarchical $MoSe_2$@g-C_3N_4 heterojunctions, *J. Mater. Chem. A*, 2021, **9**, 2742–2753.

27 S. Lin, Y. Chen, J. Fu, L. Sun, Q. Jiang, J.-F. Li, J. Cheng, C. Lin and Z.-Q. Tian, Photoelectrocatalytic nitrogen fixation with Vo-BiOBr/TiO_2 heterostructured photoelectrode as photocatalyst, *Int. J. Hydrogen Energy*, 2022, **47**, 41553–41563.

28 H. Chen, J. Liang, K. Dong, L. Yue, T. Li, Y. Luo, Z. Feng, N. Li, M. S. Hamdy, A. A. Alshehri, Y. Wang, X. Sun and Q. Liu, Ambient electrochemical N_2-to-NH_3 conversion catalyzed by TiO_2 decorated juncus effusus-derived carbon microtubes, *Inorg. Chem. Front.*, 2022, **9**, 1514–1519.

29 M. Nazemi and M. A. El-Sayed, Managing the nitrogen cycle via plasmonic (photo)electrocatalysis: toward circular economy, *Acc. Chem. Res.*, 2021, **54**, 4294–4304.

30 T. Oshikiri, K. Ueno and H. Misawa, Plasmon-induced ammonia synthesis through nitrogen photofixation with visible light irradiation, *Angew. Chem., Int. Ed.*, 2014, **53**, 9802–9805.

31 J. Wang, Z. Zhang, S. Qi, Y. Fan, Y. Yang, W. Li and M. Zhao, Photo-assisted high performance single atom electrocatalysis of the N_2 reduction reaction by a Mo-embedded covalent organic framework, *J. Mater. Chem. A*, 2021, **9**, 19949–19957.

32 M. Fritz, S. Rupp, C. I. Kiene, S. Kisan, J. Telser, C. Wurtele, V. Krewald and S. Schneider, Photoelectrochemical conversion of dinitrogen to benzonitrile: selectivity control by electrophile- versus proton-coupled electron transfer, *Angew. Chem., Int. Ed.*, 2022, **61**, e202205922.

33 H. Liang, J. Li and Y. Tian, Construction of full-spectrum-driven Ag–g-C_3N_4/$W_{18}O_{49}$ heterojunction catalyst with outstanding N_2 photofixation ability, *RSC Adv.*, 2017, **7**, 42997–43004.

34 H. Liang, H. Zou and S. Hu, Preparation of the $W_{18}O_{49}$/g-C_3N_4 heterojunction catalyst with full-spectrum-driven photocatalytic N_2 photofixation ability from the UV to near infrared region, *New J. Chem.*, 2017, **41**, 8920–8926.

35 Y.-G. Liu, M. Tian, J. Hou and H.-Y. Jiang, Research progress and perspectives on active sites of photo- and electrocatalytic nitrogen reduction, *Energy Fuels*, 2022, **36**, 11323–11358.

36 H.-J. Chen, Z.-Q. Xu, S. Sun, Y. Luo, Q. Liu, M. S. Hamdy, Z.-S. Feng, X. Sun and Y. Wang, Plasma-etched Ti_2O_3 with oxygen vacancies for enhanced NH_3 electrosynthesis and Zn–N_2 batteries, *Inorg. Chem. Front.*, 2022, **9**, 4608–4613.

37 C. Ling, X. Niu, Q. Li, A. Du and J. Wang, Metal-free single atom catalyst for N_2 fixation driven by visible light, *J. Am. Chem. Soc.*, 2018, **140**, 14161–14168.

38 M.-A. Légaré, G. Bélanger-Chabot, R. D. Dewhurst, E. Welz, I. Krummenacher, B. Engels and H. Braunschweig, Nitrogen fixation and reduction at boron, *Science*, 2018, **359**, 896–900.

39 B. Xu, H. Beckers, H. Ye, Y. Lu, J. Cheng, X. Wang and S. Riedel, Cleavage of the N identical with N triple Bond and unpredicted formation of the cyclic 1,3-diaza-2,4-diborete $(FB)_2$ N_2 from N_2 and fluoroborylene BF, *Angew. Chem., Int. Ed.*, 2021, **60**, 17205–17210.

40 J. Yu, S. Xiong, B. Wang, R. Wang, B. He, J. Jin, H. Wang and Y. Gong, Constructing boron-doped graphitic carbon nitride with 2D/1D porous hierarchical architecture and efficient N_2 photofixation, *Colloids Surf., A*, 2023, **656**, 130481.

41 L. Shi, Y. Yin, S. Wang and H. Sun, Rational catalyst design for N_2 reduction under ambient conditions: strategies toward enhanced conversion efficiency, *ACS Catal.*, 2020, **10**, 6870–6899.

42 J. Li, X. Zhu, T. Wang, Y. Luo and X. Sun, An Fe_2O_3 nanoparticle-reduced graphene oxide composite for ambient electrocatalytic N_2 reduction to NH_3, *Inorg. Chem. Front.*, 2019, **6**, 2682–2685.

43 M. Wang, S. Liu, T. Qian, J. Liu, J. Zhou, H. Ji, J. Xiong, J. Zhong and C. Yan, Over 56.55% Faradaic efficiency of ambient ammonia synthesis enabled by positively shifting the reaction potential, *Nat. Commun.*, 2019, **10**, 341.

44 M. Nazemi, S. R. Panikkanvalappil and M. A. El-Sayed, Enhancing the rate of electrochemical nitrogen reduction reaction for ammonia synthesis under ambient conditions using hollow gold nanocages, *Nano Energy*, 2018, **49**, 316–323.

45 X. Shen, S. Liu, X. Xia, M. Wang, H. Ji, Z. Wang, J. Liu, X. Zhang, C. Yan and T. Qian, Interfacial microextraction boosting nitrogen feed for efficient ambient ammonia

synthesis in aqueous electrolyte, *Adv. Funct. Mater.*, 2022, **32**, 2109422.

46 B. G. K. Rambabu, A. Hai, N. Ponpandian, J. E. Schmidt, D. D. Dionysiou, M. A. Haija and F. Banat, Dual-functional paired photoelectrocatalytic system for the photocathodic reduction of CO_2 to fuels and the anodic oxidation of furfural to value-added chemicals, *Appl. Catal., B*, 2021, **298**, 120520.

47 X. X. Jiang, X. De Hu, M. Tarek, P. Saravanan, R. Alqadhi, S. Y. Chin and M. M. Rahman, Tailoring the properties of g-C_3N_4 with CuO for enhanced photoelectrocatalytic CO_2 reduction to methanol, *J. CO2 Util.*, 2020, **40**, 101222.

48 D. Liu, J. Wang, S. Bian, Q. Liu, Y. Gao, X. Wang, P. K. Chu and X. F. Yu, Photoelectrochemical synthesis of ammonia with black phosphorus, *Adv. Funct. Mater.*, 2020, **30**, 2002731.

49 Y. J. Jang, A. E. Lindberg, M. A. Lumley and K.-S. Choi, Photoelectrochemical nitrogen reduction to ammonia on cupric and cuprous oxide photocathodes, *ACS Energy Lett.*, 2020, **5**, 1834–1839.

50 P. Li, T. Zhang, M. A. Mushtaq, S. Wu, X. Xiang and D. Yan, Research progress in organic synthesis by means of photoelectrocatalysis, *Chem. Rec.*, 2021, 841–857.

51 P. B. Pati, R. W. Wang, E. Boutin, S. Diring, S. Jobic, N. Barreau, F. Odobel and M. Robert, Photocathode functionalized with a molecular cobalt catalyst for selective carbon dioxide reduction in water, *Nat. Commun.*, 2020, **11**, 3499.

52 Y. Bai, H. Bai, Z. Fang, X. Li, W. Fan and W. Shi, Understanding the Z-scheme heterojunction of $BiVO_4$/PANI for photoelectrochemical nitrogen reduction, *Chem. Commun.*, 2021, **57**, 10568–10571.

53 M. Zhang, X. Xuan, W. Wang, C. Ma and Z. Lin, Anode photovoltage compensation–enabled synergistic CO_2 photoelectrocatalytic reduction on a flower–like graphene–decorated Cu foam cathode, *Adv. Funct. Mater.*, 2020, **30**, 2005983.

54 Y. Zhao, G. Brocks, H. Genuit, R. Lavrijsen, M. A. Verheijen and A. Bieberle-Hütter, Boosting the performance of WO_3/n–Si heterostructures for photoelectrochemical water splitting: from the role of Si to interface engineering, *Adv. Energy Mater.*, 2019, **9**, 1900940.

55 S. Y. Chae, J. Y. Choi, Y. Kim, D. Le Tri Nguyen and O. S. Joo, Photoelectrochemical CO_2 reduction with a rhenium organometallic redox mediator at semiconductor/aqueous liquid junction interfaces, *Angew. Chem., Int. Ed.*, 2019, **58**, 16395–16399.

56 H. E. Kim, J. Kim, E. C. Ra, H. Zhang, Y. J. Jang and J. S. Lee, Photoelectrochemical nitrate reduction to ammonia on ordered silicon nanowire array photocathodes, *Angew. Chem., Int. Ed.*, 2022, **61**, e202204117.

57 C. Li, T. Wang, Z. J. Zhao, W. Yang, J. F. Li, A. Li, Z. Yang, G. A. Ozin and J. Gong, Promoted fixation of molecular nitrogen with surface oxygen vacancies on plasmon-enhanced TiO_2 photoelectrodes, *Angew. Chem., Int. Ed.*, 2018, **57**, 5278–5282.

58 S. Zhou, K. Sun, C. Y. Toe, J. Yin, J. Huang, Y. Zeng, D. Zhang, W. Chen, O. F. Mohammed, X. Hao and R. Amal, Engineering a kesterite-based photocathode for photoelectrochemical ammonia synthesis from NOx reduction, *Adv. Mater.*, 2022, **34**, e2201670.

59 T. Oshikiri, K. Ueno and H. Misawa, Selective dinitrogen conversion to ammonia using water and visible light through plasmon-induced charge separation, *Angew. Chem., Int. Ed.*, 2016, **55**, 3942–3946.

60 P. Zhou, Y. Chao, F. Lv, J. Lai, K. Wang and S. Guo, Designing noble metal single-atom-loaded two-dimension photocatalyst for N_2 and CO_2 reduction via anion vacancy engineering, *Sci. Bull.*, 2020, **65**, 720–725.

61 H. Li, J. Li, Z. Ai, F. Jia and L. Zhang, Durch sauerstoffleerstellen vermittelte photokatalyse mit BiOCl: reaktivität, selektivität und ausblick, *Angew. Chem., Int. Ed.*, 2018, **130**, 128–145.

62 Y. Nosaka, M. Matsushita, J. Nishino and A. Nosaka, Nitrogen-doped titanium dioxide photocatalysts for visible response prepared by using organic compounds, *Sci. Technol. Adv. Mater.*, 2016, **6**, 143–148.

63 X. Xue, R. Chen, H. Chen, Y. Hu, Q. Ding, Z. Liu, L. Ma, G. Zhu, W. Zhang, Q. Yu, J. Liu, J. Ma and Z. Jin, Oxygen vacancy engineering promoted photocatalytic ammonia synthesis on ultrathin two-dimensional bismuth oxybromide nanosheets, *Nano Lett.*, 2018, **18**, 7372–7377.

64 Y. Mao, H. Zhang, W. Jiang, R. Zhao, Y. Liu, Z. Wang, P. Wang, Z. Zheng, K. Song, W. Wei, Y. Dai, J.-H. He, H. Cheng and B. Huang, An integrated Si photocathode with lithiation-activated molybdenum oxide nanosheets for efficient ammonia synthesis, *Nano Energy*, 2022, **102**, 107639.

65 D. Zhang, J. Li, Q. Wang and Q. Wu, High {001} facets dominated BiOBr lamellas: facile hydrolysis preparation and selective visible-light photocatalytic activity, *J. Mater. Chem. A*, 2013, **1**, 8622–8629.

66 D. Liu, D. Chen, N. Li, Q. Xu, H. Li, J. He and J. Lu, Surface engineering of g-C_3N_4 by stacked BiOBr sheets rich in oxygen vacancies for boosting photocatalytic performance, *Angew. Chem., Int. Ed.*, 2020, **59**, 4519–4524.

67 Y. Zhao, L. Zheng, R. Shi, S. Zhang, X. Bian, F. Wu, X. Cao, G. I. N. Waterhouse and T. Zhang, Alkali etching of layered double hydroxide nanosheets for enhanced photocatalytic N2 reduction to NH3, *Adv. Energy Mater.*, 2020, **10**, 2002199.

68 M. Li, Q. Lu, M. Liu, P. Yin, C. Wu, H. Li, Y. Zhang and S. Yao, Photoinduced charge separation via the double-electron transfer mechanism in nitrogen vacancies g-C_3N_5/BiOBr for the photoelectrochemical nitrogen reduction, *ACS Appl. Mater. Interfaces*, 2020, **12**, 38266–38274.

69 M. Soleilhavoup and G. Bertrand, Borylenes: an emerging class of compounds, *Angew. Chem., Int. Ed.*, 2017, **56**, 10282–10292.

70 P. X. Sun, Z. Cao, Y. X. Zeng, W. W. Xie, N. W. Li, D. Luan, S. Yang, L. Yu and X. W. D. Lou, Formation of super-

assembled $TiO_{(x)}$/Zn/N-doped carbon inverse opal towards dendrite-free Zn anodes, *Angew. Chem., Int. Ed.*, 2022, **61**, e202115649.

71 G. N. Schrauzer and T. D. Guth, Photolysis of water and photoreduction of nitrogen on titanium dioxide, *J. Am. Chem. Soc.*, 1977, **99**, 7189–7193.

72 F. Xu, F. Wu, K. Zhu, Z. Fang, D. Jia, Y. Wang, G. Jia, J. Low, W. Ye, Z. Sun, P. Gao and Y. Xiong, Boron doping and high curvature in Bi nanorolls for promoting photoelectrochemical nitrogen fixation, *Appl. Catal., B*, 2021, **284**, 119689.

73 M. Lv, X. Sun, S. Wei, C. Shen, Y. Mi and X. Xu, Ultrathin lanthanum tantalate perovskite nanosheets modified by nitrogen doping for efficient photocatalytic water splitting, *ACS Nano*, 2017, **11**, 11441–11448.

74 J. Cao, N. Li and X. Zeng, Exploring the synergistic effect of B–N doped defective graphdiyne for N_2 fixation, *New J. Chem.*, 2021, **45**, 6327–6335.

75 X. Yu, P. Han, Z. Wei, L. Huang, Z. Gu, S. Peng, J. Ma and G. Zheng, Boron-doped graphene for electrocatalytic N_2 reduction, *Joule*, 2018, **2**, 1610–1622.

76 Y. Li, Y. Zhao, H. Cheng, Y. Hu, G. Shi, L. Dai and L. Qu, Nitrogen-doped graphene quantum dots with oxygen-rich functional groups, *J. Am. Chem. Soc.*, 2012, **134**, 15–18.

77 P. Zhai, T. C. Wei, Y. H. Chang, Y. T. Huang, W. T. Yeh, H. Su and S. P. Feng, High electrocatalytic and wettable nitrogen-doped microwave-exfoliated graphene nanosheets as counter electrode for dye-sensitized solar cells, *Small*, 2014, **10**, 3347–3353.

78 X. Peng, D. Chen, X. Yang, D. Wang, M. Li, C. C. Tseng, R. Panneerselvam, X. Wang, W. Hu, J. Tian and Y. Zhao, Microwave-assisted synthesis of highly dispersed PtCu nanoparticles on three-dimensional nitrogen-doped graphene networks with remarkably enhanced methanol electrooxidation, *ACS Appl. Mater. Interfaces*, 2016, **8**, 33673–33680.

79 N.-I. Kim, R. A. Afzal, S. R. Choi, S. W. Lee, D. Ahn, S. Bhattacharjee, S.-C. Lee, J. H. Kim and J.-Y. Park, Highly active and durable nitrogen doped-reduced graphene oxide/double perovskite bifunctional hybrid catalysts, *J. Mater. Chem. A*, 2017, **5**, 13019–13031.

80 L. Paramanik, S. Sultana and K. M. Parida, Photocatalytic and photo-electrochemical ammonia synthesis over dimensional oriented cobalt titanate/nitrogen-doped reduced graphene oxide junction interface catalyst, *J. Colloid Interface Sci.*, 2022, **625**, 83–99.

81 C. Dai, Y. Huang and J. Zhu, Predicting dinitrogen activation by carborane-based frustrated lewis pairs, *Organometallics*, 2022, **41**, 1480–1487.

82 C. Tang, Q. Liang, A. R. Jupp, T. C. Johnstone, R. C. Neu, D. Song, S. Grimme and D. W. Stephan, 1,1-hydroboration and a borane adduct of diphenyldiazomethane: a potential prelude to FLP-N_2 chemistry, *Angew. Chem., Int. Ed.*, 2017, **56**, 16588–16592.

83 W. Lin, H. Chen, G. Lin, S. Yao, Z. Zhang, J. Qi, M. Jing, W. Song, J. Li, X. Liu, J. Fu and S. Dai, Creating frustrated lewis pairs in defective boron carbon nitride for electrocatalytic nitrogen reduction to ammonia, *Angew. Chem., Int. Ed.*, 2022, **61**, e202207807.

84 Z. Chen, J. Zhao, Y. Jiao, T. Wang and L. Yin, Achieving efficient N_2 electrochemical reduction by stabilizing the N_2H^* intermediate with the frustrated Lewis pairs, *J. Energy Chem.*, 2022, **66**, 628–634.

85 M. Yuan, J. Chen, Y. Xu, R. Liu, T. Zhao, J. Zhang, Z. Ren, Z. Liu, C. Streb, H. He, C. Yang, S. Zhang and G. Zhang, Highly selective electroreduction of N_2 and CO_2 to urea over artificial frustrated Lewis pairs, *Energy Environ. Sci.*, 2021, **14**, 6605–6615.

86 R. L. Melen, A step closer to metal-free dinitrogen activation: a new chapter in the chemistry of frustrated Lewis pairs, *Angew. Chem., Int. Ed.*, 2018, **57**, 880–882.

87 Y. Ran, X. Yu, J. Liu, J. Cui, J. Wang, L. Wang, Y. Zhang, X. Xiang and J. Ye, Polymeric carbon nitride with frustrated Lewis pair sites for enhanced photofixation of nitrogen, *J. Mater. Chem. A*, 2020, **8**, 13292–13298.

88 L. Chen, J. Wang, X. Li, C. Zhao, X. Hu, Y. Wu and Y. He, A novel Z-scheme Bi-Bi_2O_3/$KTa_{0.5}Nb_{0.5}O_3$ heterojunction for efficient photocatalytic conversion of N_2 to NH_3, *Inorg. Chem. Front.*, 2022, **9**, 2714–2724.

89 R. Marschall, Semiconductor composites: strategies for enhancing charge carrier separation to improve photocatalytic activity, *Adv. Funct. Mater.*, 2014, **24**, 2421–2440.

90 M. Asadi, K. Kim, C. Liu, A. V. Addepalli, P. Abbasi, P. Yasaei, P. Phillips, A. Behranginia, J. M. Cerrato, R. Haasch, P. Zapol, B. Kumar, R. F. Klie, J. Abiade, L. A. Curtiss and A. Salehi-Khojin, Nanostructured transition metal dichalcogenide electrocatalysts for CO_2 reduction in ionic liquid, *Science*, 2016, **353**, 467–470.

91 J. Liang, Q. Liu, A. A. Alshehri and X. Sun, Recent advances in nanostructured heterogeneous catalysts for N-cycle electrocatalysis, *Nano Res. Energy*, 2022, **1**, e9120010.

92 S. Zhao, Y. Wang, J. Dong, C.-T. He, H. Yin, P. An, K. Zhao, X. Zhang, C. Gao, L. Zhang, J. Lv, J. Wang, J. Zhang, A. M. Khattak, N. A. Khan, Z. Wei, J. Zhang, S. Liu, H. Zhao and Z. Tang, Ultrathin metal–organic framework nanosheets for electrocatalytic oxygen evolution, *Nat. Energy*, 2016, **1**, 16184.

93 L. Feng, S. Yuan, L. L. Zhang, K. Tan, J. L. Li, A. Kirchon, L. M. Liu, P. Zhang, Y. Han, Y. J. Chabal and H. C. Zhou, Creating hierarchical pores by controlled linker thermolysis in multivariate metal-organic frameworks, *J. Am. Chem. Soc.*, 2018, **140**, 2363–2372.

94 Y. Liu, H. Bai, Q. Zhang, Y. Bai, X. Pang, F. Wang, Y. Yang, J. Ding, W. Fan and W. Shi, In-situ decoration of unsaturated Cu sites on Cu_2O photocathode for boosting nitrogen reduction reaction, *Chem. Eng. J.*, 2021, **413**, 127453.

95 X. Li, W. Fan, Y. Bai, Y. Liu, F. Wang, H. Bai and W. Shi, Photoelectrochemical reduction of nitrate to ammonia over CuPc/CeO_2 heterostructure: Understanding the synergistic effect between oxygen vacancies and Ce sites, *Chem. Eng. J.*, 2022, **433**, 133225.

96 H. Guo, H. Zhang, J. Zhao, P. Yuan, Y. Li, Y. Zhang, L. Li, S. Wang and R. Song, Two-dimensional WO_3-transition-metal dichalcogenide vertical heterostructures for nitrogen fixation: a photo(Electro) catalysis theoretical strategy, *J. Phys. Chem. C*, 2022, **126**, 3043–3053.

97 J. Zheng, Y. Lyu, M. Qiao, R. Wang, Y. Zhou, H. Li, C. Chen, Y. Li, H. Zhou, S. P. Jiang and S. Wang, Photoelectrochemical synthesis of ammonia on the aerophilic-hydrophilic heterostructure with 37.8% efficiency, *Chem*, 2019, **5**, 617–633.

98 S. T. Gyama, Preparation and catalytic properties of transition metal carbides and nitrides, *Catal. Today*, 1992, **15**, 179–200.

99 X. Li, M. Deng, W. Zhang, Q. Gao, H. Wang, B. Yuan, L. Yang and M. Zhu, Mo2C/N-doped carbon nanowires as anode materials for sodium-ion batteries, *Mater. Lett.*, 2017, **194**, 30–33.

100 L. Liu, W. An, H. Wang, H. Guo, Y. Liang and W. Cui, Ultrathin porous g-C_3N_4 nanosheets modified with AuCu alloy nanoparticles and C-C coupling photothermal catalytic reduction of CO_2 to ethanol, *Appl. Catal., B*, 2020, **266**, 118618.

101 F. You, J. Wan, J. Qi, D. Mao, N. Yang, Q. Zhang, L. Gu and D. Wang, Lattice distortion in hollow multi-shelled structures for efficient visible-light CO_2 reduction with a SnS_2/SnO_2 Junction, *Angew. Chem., Int. Ed.*, 2020, **59**, 721–724.

102 M. Luo, Y. Sun, L. Wang and S. Guo, Tuning multimetallic ordered intermetallic nanocrystals for efficient energy electrocatalysis, *Adv. Energy Mater.*, 2017, **7**, 1602073.

103 G. Yasin, S. Ibraheem, S. Ali, M. Arif, S. Ibrahim, R. Iqbal, A. Kumar, M. Tabish, M. A. Mushtaq, A. Saad, H. Xu and W. Zhao, Defects-engineered tailoring of tri-doped interlinked metal-free bifunctional catalyst with lower gibbs free energy of OER/HER intermediates for overall water splitting, *Mater. Today Chem.*, 2022, **23**, 100634.

104 M. A. Mushtaq, A. Kumar, G. Yasin, M. Arif, M. Tabish, S. Ibraheem, X. Cai, W. Ye, X. Fang, A. Saad, J. Zhao, S. Ji and D. Yan, 3D interconnected porous Mo-doped WO_3@CdS hierarchical hollow heterostructures for efficient photoelectrochemical nitrogen reduction to ammonia, *Appl. Catal., B*, 2022, **317**, 121711.

105 Y. Zhao, Y. Zhao, G. I. N. Waterhouse, L. Zheng, X. Cao, F. Teng, L. Z. Wu, C. H. Tung, D. O'Hare and T. Zhang, Layered-double-hydroxide nanosheets as efficient visible-light-driven photocatalysts for dinitrogen fixation, *Adv. Mater.*, 2017, **29**, 1703828.

106 M. Arif, G. Yasin, L. Luo, W. Ye, M. A. Mushtaq, X. Fang, X. Xiang, S. Ji and D. Yan, Hierarchical hollow nanotubes of NiFeV-layered double hydroxides@CoVP heterostructures towards efficient, pH-universal electrocatalytical nitrogen reduction reaction to ammonia, *Appl. Catal., B*, 2020, **265**, 118559.

107 S. Koynov, M. S. Brandt and M. Stutzmann, Black nonreflecting silicon surfaces for solar cells, *Appl. Phys. Lett.*, 2006, **88**, 203107.

108 J. Oh, H. C. Yuan and H. M. Branz, An 18.2%-efficient black-silicon solar cell achieved through control of carrier recombination in nanostructures, *Nat. Nanotechnol.*, 2012, **7**, 743–748.

109 K. Peramaiah, V. Ramalingam, H. C. Fu, M. M. Alsabban, R. Ahmad, L. Cavallo, V. Tung, K. W. Huang and J. H. He, Optically and electrocatalytically decoupled Si photocathodes with a porous carbon nitride catalyst for nitrogen reduction with over 61.8% faradaic efficiency, *Adv. Mater.*, 2021, **33**, e2100812.

110 H. Yang, C. Nan, N. Gao, W. Zhou, F. Gao, D. Dong, D. Dou, Y. Liu, Z. Liang and D. Yang, Three-phase interface of SnO_2 nanoparticles loaded on hydrophobic MoS_2 enhance photoelectrochemical N_2 reduction, *Electrochim. Acta*, 2022, **430**, 141086.

111 N. Gao, H. Yang, D. Dong, D. Dou, Y. Liu, W. Zhou, F. Gao, C. Nan, Z. Liang and D. Yang, Bi_2S_3 quantum dots in situ grown on MoS_2 nanoflowers: an efficient electron-rich interface for photoelectrochemical N_2 reduction, *J. Colloid Interface Sci.*, 2022, **611**, 294–305.

112 W. Ye, M. Arif, X. Fang, M. A. Mushtaq, X. Chen and D. Yan, Efficient photoelectrochemical route for the ambient reduction of N_2 to NH_3 based on nanojunctions assembled from MoS_2 nanosheets and TiO_2, *ACS Appl. Mater. Interfaces*, 2019, **11**, 28809–28817.

113 X. Xu, X. Tian, B. Sun, Z. Liang, H. Cui, J. Tian and M. Shao, 1 T-phase molybdenum sulfide nanodots enable efficient electrocatalytic nitrogen fixation under ambient conditions, *Appl. Catal., B*, 2020, **272**, 118984.

114 X. Li, H. Liu, D. Luo, J. Li, Y. Huang, H. Li, Y. Fang, Y. Xu and L. Zhu, Adsorption of CO_2 on heterostructure CdS (Bi_2S_3)/TiO_2 nanotube photocatalysts and their photocatalytic activities in the reduction of CO_2 to methanol under visible light irradiation, *Chem. Eng. J.*, 2012, **180**, 151–158.

115 Y. Hu, Z. L. Zhao, R. Ahmad, M. Harb, L. Cavallo, L. M. Azofra, S. P. Jiang and X. Zhang, A bifunctional catalyst based on a carbon quantum dots/mesoporous $SrTiO_3$ heterostructure for cascade photoelectrochemical nitrogen reduction, *J. Mater. Chem. A*, 2022, **10**, 12713–12721.

116 X. Li, P. Shen, Y. Luo, Y. Li, Y. Guo, H. Zhang and K. Chu, PdFe single-atom alloy metallene for N_2 electroreduction, *Angew. Chem., Int. Ed.*, 2022, **61**, e202205923.

117 C. Kim, J. Y. Song, C. Choi, J. P. Ha, W. Lee, Y. T. Nam, D. M. Lee, G. Kim, I. Gereige, W. B. Jung, H. Lee, Y. Jung, H. Jeong and H. T. Jung, Atomic-scale homogeneous Ru–Cu alloy nanoparticles for highly efficient electrocatalytic nitrogen reduction, *Adv. Mater.*, 2022, **34**, e2205270.

118 H. L. Du, M. Chatti, R. Y. Hodgetts, P. V. Cherepanov, C. K. Nguyen, K. Matuszek, D. R. MacFarlane and A. N. Simonov, Electroreduction of nitrogen with almost 100% current-to-ammonia efficiency, *Nature*, 2022, **609**, 722–727.

119 H.-L. Du, K. Matuszek, R. Y. Hodgetts, K. N. Dinh, P. V. Cherepanov, J. M. Bakker, D. R. MacFarlane and

A. N. Simonov, The chemistry of proton carriers in high-performance lithium-mediated ammonia electrosynthesis, *Energy Environ. Sci.*, 2023, **16**, 1082–1090.

120 R. Karimi, F. Yousefi, M. Ghaedi, K. Dashtian and G. Yasin, Unveiling charge dynamics of Co_3S_4 nanowalls/CdS nanospheres n-n heterojunction for efficient photoelectrochemical Cr(VI) detoxification and N_2 fixation, *J. Environ. Chem. Eng.*, 2022, **10**, 108549.

121 X. Li, W. Fan, D. Xu, J. Ding, H. Bai and W. Shi, Boosted photoelectrochemical N_2 reduction over Mo_2C in situ coated with graphitized carbon, *Langmuir*, 2020, **36**, 14802–14810.

122 Y. Abghoui, A. L. Garden, J. G. Howalt, T. Vegge and E. Skúlason, Electroreduction of N_2 to ammonia at ambient conditions on mononitrides of Zr, Nb, Cr, and V: A DFT guide for experiments, *ACS Catal.*, 2015, **6**, 635–646.

123 Z. Geng, Y. Liu, X. Kong, P. Li, K. Li, Z. Liu, J. Du, M. Shu, R. Si and J. Zeng, Achieving a record-high yield rate of 120.9 mug NH_3 $mg_{cat.}^{-1}$ h^{-1} for N2 electrochemical reduction over Ru single-atom catalysts, *Adv. Mater.*, 2018, e1803498.

124 B. H. R. Suryanto, C. S. M. Kang, D. Wang, C. Xiao, F. Zhou, L. M. Azofra, L. Cavallo, X. Zhang and D. R. MacFarlane, Rational electrode–electrolyte design for efficient ammonia electrosynthesis under ambient conditions, *ACS Energy Lett.*, 2018, **3**, 1219–1224.

125 T. B. Yuan, Z. Hu, Y. X. Zhao, J. J. Fang, J. Lv, Q. H. Zhang, Z. B. Zhuang, L. Gu and S. Hu, Two-dimensional amorphous SnOx from liquid metal: mass production, phase transfer, and electrocatalytic CO2 reduction toward formic acid, *Nano Lett.*, 2020, **20**, 2916–2922.

126 C. Xu, X. Zhang, M.-N. Zhu, L. Zhang, P.-F. Sui, R. Feng, Y. Zhang and J.-L. Luo, Accelerating photoelectric CO2 conversion with a photothermal wavelength-dependent plasmonic local field, *Appl. Catal., B*, 2021, **298**, 120533.

127 M. P. Kou, W. Liu, Y. Y. Wang, J. D. Huang, Y. L. Chen, Y. Zhou, Y. Chen, M. Z. Ma, K. Lei, H. Q. Xie, P. K. Wong and L. Q. Ye, Photocatalytic CO_2 conversion over single-atom MoN2 sites of covalent organic framework, *Appl. Catal., B*, 2021, **291**, 120146.

128 L. Li, C. Tang, B. Xia, H. Jin, Y. Zheng and S.-Z. Qiao, Two-dimensional mosaic bismuth nanosheets for highly selective ambient electrocatalytic nitrogen reduction, *ACS Catal.*, 2019, **9**, 2902–2908.

129 X. Yang, J. Nash, J. Anibal, M. Dunwell, S. Kattel, E. Stavitski, K. Attenkofer, J. G. Chen, Y. Yan and B. Xu, Mechanistic insights into electrochemical nitrogen reduction reaction on vanadium nitride nanoparticles, *J. Am. Chem. Soc.*, 2018, **140**, 13387–13391.

130 Y. Yao, H. Wang, X.-Z. Yuan, H. Li and M. Shao, Electrochemical nitrogen reduction reaction on ruthenium, *ACS Energy Lett.*, 2019, **4**, 1336–1341.

131 H. Feng, Z. Xu, L. Ren, C. Liu, J. Zhuang, Z. Hu, X. Xu, J. Chen, J. Wang, W. Hao, Y. Du and S. X. Dou, Activating titania for efficient electrocatalysis by vacancy engineering, *ACS Catal.*, 2018, **8**, 4288–4293.

132 Z. Yan, M. Ji, J. Xia and H. Zhu, Recent advanced materials for electrochemical and photoelectrochemical synthesis of ammonia from dinitrogen: one step closer to a sustainable energy future, *Adv. Energy Mater.*, 2019, **10**, 1922020.

133 J. Zheng, Y. Lyu, J.-P. Veder, B. Johannessen, R. Wang, R. De Marco, A. Huang, S. P. Jiang and S. Wang, Electrochemistry-assisted photoelectrochemical reduction of nitrogen to ammonia, *J. Phys. Chem. C*, 2021, **125**, 23041–23049.

134 A. R. Singh, B. A. Rohr, J. A. Schwalbe, M. Cargnello, K. Chan, T. F. Jaramillo, I. Chorkendorff and J. K. Nørskov, Electrochemical ammonia synthesis—the selectivity challenge, *ACS Catal.*, 2016, **7**, 706–709.

135 D. V. Yandulov and R. R. Schrock, Catalytic reduction of dinitrogen to ammonia at a single molybdenum center, *Science*, 2003, **301**, 76–78.

136 H. K. Lee, C. S. L. Koh, Y. H. Lee, C. Liu, I. Y. Phang, X. Han, C.-K. Tsung and X. Y. Ling, Favoring the unfavored: selective electrochemical nitrogen fixation using a reticular chemistry approach, *Sci. Adv.*, 2018, **4**, eaar3208.

137 P. J. Hill, L. R. Doyle, A. D. Crawford, W. K. Myers and A. E. Ashley, Selective catalytic reduction of N_2 to N_2H_4 by a simple Fe complex, *J. Am. Chem. Soc.*, 2016, **138**, 13521–13524.

138 Y. Abghoui, A. L. Garden, V. F. Hlynsson, S. Bjorgvinsdottir, H. Olafsdottir and E. Skulason, Enabling electrochemical reduction of nitrogen to ammonia at ambient conditions through rational catalyst design, *Phys. Chem. Chem. Phys.*, 2015, **17**, 4909–4918.

139 H. Ali, M. Masar, A. C. Guler, M. Urbanek, M. Machovsky and I. Kuritka, Heterojunction-based photocatalytic nitrogen fixation: principles and current progress, *Nanoscale Adv.*, 2021, **3**, 6358–6372.

140 N. Zhang, L. Li, Q. Shao, T. Zhu, X. Huang and X. Xiao, Fe-doped BiOCl nanosheets with light-switchable oxygen vacancies for photocatalytic nitrogen fixation, *ACS Appl. Energy Mater.*, 2019, **2**, 8394–8398.

141 T. Wang, C. Feng, J. Liu, D. Wang, H. Hu, J. Hu, Z. Chen and G. Xue, Bi_2WO_6 hollow microspheres with high specific surface area and oxygen vacancies for efficient photocatalysis N_2 fixation, *Chem. Eng. J.*, 2021, **414**, 128827.

142 K. Hu, Z. Huang, L. Zeng, Z. Zhang, L. Mei, Z. Chai and W. Shi, Recent advances in MOF–based materials for photocatalytic nitrogen fixation, *Eur. J. Inorg. Chem.*, 2021, **2022**, e202100748.

143 D. Yan, H. Li, C. Chen, Y. Zou and S. Wang, Defect engineering strategies for nitrogen reduction reactions under ambient conditions, *Small Methods*, 2018, **3**, 1800331.

144 A. C. Nielander, J. M. McEnaney, J. A. Schwalbe, J. G. Baker, S. J. Blair, L. Wang, J. G. Pelton, S. Z. Andersen, K. Enemark-Rasmussen, V. Čolić, S. Yang, S. F. Bent, M. Cargnello, J. Kibsgaard, P. C. K. Vesborg,

I. Chorkendorff and T. F. Jaramillo, A versatile method for ammonia detection in a range of relevant electrolytes via direct nuclear magnetic resonance techniques, *ACS Catal.*, 2019, **9**, 5797–5802.

145 Y.-C. Hao, Y. Guo, L.-W. Chen, M. Shu, X.-Y. Wang, T.-A. Bu, W.-Y. Gao, N. Zhang, X. Su, X. Feng, J.-W. Zhou, B. Wang, C.-W. Hu, A.-X. Yin, R. Si, Y.-W. Zhang and C.-H. Yan, Promoting nitrogen electroreduction to ammonia with bismuth nanocrystals and potassium cations in water, *Nat. Catal.*, 2019, **2**, 448–456.

146 Y. Zhao, R. Shi, X. Bian, C. Zhou, Y. Zhao, S. Zhang, F. Wu, G. I. N. Waterhouse, L. Z. Wu, C. H. Tung and T. Zhang, Ammonia detection methods in photocatalytic and electrocatalytic experiments: how to improve the reliability of NH_3 production rates?, *Adv. Sci.*, 2019, **6**, 1802109.

147 J. Yuan, X. Yi, Y. Tang, M. Liu and C. Liu, Efficient photocatalytic nitrogen fixation: enhanced polarization, activation, and cleavage by asymmetrical electron donation to N≡N bond, *Adv. Funct. Mater.*, 2019, **30**, 1906983.

148 A. LeDuy and R. Samson, Testing of an ammonia ion selective electrode for ammonia nirogen measureture in the methanogenic sludge, *Biotechnol. Lett.*, 1982, **4**, 303–306.

149 H. Wang, L. Wang, Q. Wang, S. Ye, W. Sun, Y. Shao, Z. Jiang, Q. Qiao, Y. Zhu, P. Song, D. Li, L. He, X. Zhang, J. Yuan, T. Wu and G. A. Ozin, Ambient electrosynthesis of ammonia: electrode porosity and composition engineering, *Angew. Chem., Int. Ed.*, 2018, **57**, 12360–12364.